POLITECNICO DI TORINO
Repository ISTITUZIONALE

The component-wise to evaluate homogenized methods in layer-wise approaches for honeycomb sandwich panels

Original
The component-wise to evaluate homogenized methods in layer-wise approaches for honeycomb sandwich panels / Carrera, E., Salem, K.A., Augello, R.. - In: COMPOSITE STRUCTURES. - ISSN 0263-8223. - 374:(2025). [10.1016/j.compstruct.2025.119740]

Availability:
This version is available at: 11583/3017460 since: 2026-11-03T11:03:59Z

Publisher:
Elsevier

Published
DOI:10.1016/j.compstruct.2025.119740

Terms of use:

This article is made available under terms and conditions as specified in the corresponding bibliographic description in the repository

Publisher copyright

(Article begins on next page)

07 November 2026

Composite Structures 374 (2025) 119740



Contents lists available at ScienceDirect

Composite Structures

journal homepage: www.elsevier.com/locate/compstruct





The component-wise to evaluate homogenized methods in layer-wise approaches for honeycomb sandwich panels

Erasmo Carrera *, Karim Abu Salem, Riccardo Augello

Department of Mechanical and Aerospace Engineering, Politecnico di Torino, Corso Duca degli Abruzzi 24, 10129 Torino, Italy

ARTICLE INFO

Keywords:
Honeycomb
Sandwich
Cuf
Layer-wise
Homogenization

ABSTRACT

This paper proposes an unprecedented 'component-wise' one-dimensional beam finite element model to investigate the reliability of analytical homogenization models in predicting the equivalent orthotropic properties of honeycomb cores in static and dynamic sandwich structures analyses. Classical and advanced schemes are considered, each introducing different levels of refinement in representing the mechanics of the core. Two representative honeycomb configurations are analysed to assess the sensitivity of the models to variations in cell topology, wall thickness, and boundary conditions. Equivalent properties derived from homogenization are implemented in a Layer-Wise (LW) formulation and compared against high-fidelity Component-Wise (CW) models that explicitly resolve the real core geometry. Both LW and CW approaches are formulated within the Carrera Unified Formulation, ensuring a consistent methodological framework. The study includes static analyses under bending and torsion and modal analyses. Results show that homogenized LW models can reproduce some global trends but fail to capture local effects and heterogeneous stiffness distributions, leading to significant deviations in both static and dynamic responses. By contrast, CW models consistently provide accurate predictions by preserving the intrinsic variability of the stiffness field. These findings highlight the intrinsic limitations of homogenization when applied to complex honeycomb structures and demonstrate that CW models offer a more powerful and reliable to assess actual mechanical response of sandwich panels, in the widest range of loading and boundary conditions. While homogenization remains useful for initial global assessment and preliminary design, the advancement proposed here is the recognition of CW formulations as the necessary reference to evaluate, validate, and ultimately improve homogenized approaches in the analysis of advanced and complex sandwich panels.

1. Introduction

Lightweight structural systems that combine high stiffness with reduced mass are essential in aerospace, marine, and advanced transportation sectors. Among the most effective solutions, sandwich panels with honeycomb cores offer an optimal balance between stiffness and weight efficiency [1–6]. The mechanical behaviour of these structures results from the synergy between stiff face sheets and a compliant cellular core, which ensures load transmission and out-of-plane stiffness.

Despite their extensive use, the accurately modelling of honeycomb sandwich panels remains a complex task. The core structure, composed of thin-walled periodic cells, introduces multiple interacting scales and significant geometrical details. When modelled explicitly, this leads to complex simulations and high computational costs, as in full 3D analyses [7–9]. While such high-fidelity simulations can capture local stress concentrations and interface phenomena, they are often prohibitive for early design-phase evaluations or parametric studies. To overcome these challenges, homogenization techniques are commonly employed [10–14]. These methods replace the detailed actual cellular architecture with an equivalent orthotropic continuum, defined through effective elastic constants derived analytically from the cell geometry and material properties. Several homogenization models have been proposed, ranging from early beam-based formulations to more refined treatments [15–24].

Each approach is based on a different set of assumptions, and their applicability varies significantly depending on the mechanical scenario and core configuration. However, the predictive capability of homogenized models is not clear, particularly when applied to cores with geometric irregularities, partial cells, asymmetric edge conditions, or mixed topologies. While some simplifications could be acceptable in symmetric

* Corresponding author.
E-mail addresses: erasmo.carrera@polito.it (E. Carrera), karim.abusalem@polito.it (K.A. Salem), riccardo.augello@polito.it (R. Augello).

https://doi.org/10.1016/j.compstruct.2025.119740
Received 24 August 2025; Accepted 8 October 2025
Available online 11 October 2025
0263-8223/© 2025 The Author(s). Published by Elsevier Ltd. This is an open access article under the CC BY license (http://creativecommons.org/licenses/by/4.0/).

or ideal configurations, they may lead to inaccurate or even misleading results in practical design cases where local phenomena govern the global response.

To assess the structural behaviour of sandwich panels incorporating these homogenized core properties, Carrera Unified Formulation (CUF) [25] provides a powerful modelling platform. Within this framework, both reduced-order and high-fidelity structural models can be developed. In particular, the Layer-Wise (LW) approach [26–29] allows for an efficient representation of the sandwich architecture by assigning independent displacement fields to each layer, incorporating equivalent core properties. Conversely, the Component-Wise (CW) approach [30–32] explicitly models each physical component, including individual honeycomb walls, thus preserving the full geometric and mechanical detail without the need for homogenization. Despite the wide use of homogenized theories for sandwich structures, the literature lacks a comprehensive and quantitative analysis of how different homogenization methods perform under realistic geometric conditions and structural loadings. Previous works often validate isolated models or propose alternative formulations, but the impact of the selected model or local stiffness heterogeneities on the predictive capability of reduced-order models is still weakly characterized. This defines the research gap addressed in this paper: the rigorous, comparative evaluation of analytical homogenization models for honeycomb cores, and the need to clarify their domain of applicability in structural simulations. While reduced-order methods remain attractive for design purposes, their limitations in capturing local effects is a relevant issue. Two honeycomb core configurations, regular and non-regular, are investigated under bending, torsion, and free vibration conditions. Particular attention is given to the effect of core height and skin thickness, which are shown to significantly modulate the accuracy of the reduced-order models. The results aim to define clear guidelines for when simplified modelling is acceptable, and when geometric resolution becomes essential.

2. Methodology

This section presents a comparative overview of analytical models for estimating the equivalent orthotropic properties of honeycomb cores based on their geometric features. Additionally, the section introduces the Layer-Wise and Component-Wise kinematic formulations developed within the Carrera Unified Formulation, which are used to incorporate the homogenized properties or the full geometric detail into the structural analysis of sandwich configurations.

2.1. Homogenization of honeycomb core

Analytical homogenization techniques aim to replace a geometrically complex cellular material with an equivalent continuum characterized by equivalent mechanical properties. In the case of honeycomb cores, the goal is to derive the elastic constants of an orthotropic solid that approximates the overall mechanical response of the periodic microstructure under macroscopic loading. The homogenized properties are typically functions of the geometry (cell size, wall thickness, inclination angles), base material properties, and cell topology. The models, indeed, rely on the definition of a representative cell element (RCE) that captures the geometry of the honeycomb structure, characterized by its vertical and inclined cell walls with dimensions h, l, wall thickness t, and cell angle θ, see Fig. 1. Classical approaches usually model the walls as beam or frame elements and use simplified force or displacement-based energy methods. The resulting equivalent elastic constants include in-plane Young moduli, shear moduli, and Poisson ratios, and, in some cases, out-of-plane properties when 3D behaviour is considered. Homogenization reduces computational cost and model complexity, enabling efficient structural analysis of sandwich panels while attempting to preserve acceptable accuracy. In the following the main assumptions and a general overview of some relevant homogenization models from literature are outlined.

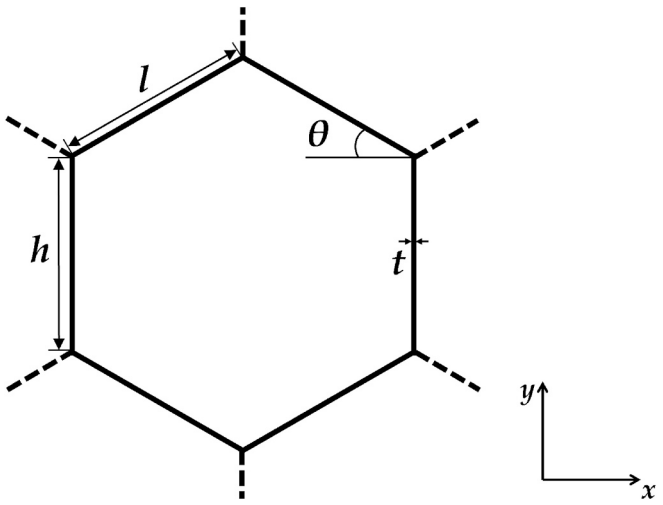


Fig. 1. RCE for a reference honeycomb core.

- **Gibson & Ashby homogenization model**

Gibson & Ashby model [15] can be considered as the main reference for the honeycomb homogenization techniques. They established a theoretical framework for cellular solids by idealizing the honeycomb core as an assembly of slender periodic cell walls. The model assumes that the mechanical response of these structures is predominantly governed by bending deformations rather than direct axial stretching. In this context, the effective behaviour of the core is derived from the geometric parameters of the cells. The derivation initiates with the analysis of an individual cell wall subjected to in-plane bending. By applying linear elastic theory, the bending stiffness of the wall is expressed in terms of the wall dimensions and the intrinsic material properties. This process leads to closed-form expressions for the equivalent orthotropic elastic moduli. A key assumption is the idealized geometry of the cells; the orthotropic nature of the derived equivalent solid directly reflects the anisotropic distribution of cell orientations inherent to the honeycomb structure. Gibson & Ashby model equations are reported in Table 1, for the nine equivalent mechanical properties. Geometric parameters l, h, t, and θ are indicated in Fig. 1, whereas E_m, G_m, and ν_m are the elastic properties of the isotropic base material, aluminum in our study cases.

- **Nast homogenization model**

Nast model [33] diverges from Gibson & Ashby by abandoning the beam idealization of cell walls in favour of a differential plate approach.

Table 1
Equivalent mechanical properties: Gibson & Ashby model.

E_x	E_y	E_z
$\frac{E_m\left(\frac{t}{l}\right)^3 cos\theta}{\left(\frac{h}{l}+sin\theta\right)sin^2\theta}$	$\frac{E_m\left(\frac{t}{l}\right)^3\left(\frac{h}{l}+sin\theta\right)}{cos^3\theta}$	$E_m\left(\frac{t}{l}\right)\frac{\left(1+\frac{h}{l}\right)}{cos\theta\left(\frac{h}{l}+sin\theta\right)}$
G_{xy}	G_{xz}	G_{yz}
$E_m\left(\frac{t}{l}\right)^3\left(\frac{h}{L}\right)^2\left(1+\frac{h}{4l}\right)\frac{1}{cos\theta}$	$G_m\left(\frac{t}{l}\right)\frac{cos\theta}{\left(\frac{h}{l}+sin\theta\right)}$	$G_m\left(\frac{t}{l}\right)\frac{\left(\frac{h}{l}+sin\theta\right)}{cos\theta\left(1+\frac{h}{l}\right)}$
ν_{xy}	ν_{xz}	ν_{yz}
$\frac{cos^2\theta}{\left(\frac{h}{l}+sin\theta\right)sin\theta}$	$\nu_m\frac{E_x}{E_z}$	$\nu_m\frac{E_y}{E_z}$

Table 2
Equivalent mechanical properties: Nast model.

E_x	E_y	E_z
$\frac{E_m}{1-\nu_m{}^2}\frac{t^3(sin\theta+1)}{12l^3cos^2\theta\left(\frac{cos\theta}{3}-\frac{1+cos\theta}{8}\right)}$	$\frac{E_m}{1-\nu_m{}^2}\frac{t^3cos\theta}{l^3sin^2\theta(1+sin\theta)}$	$E_m\left(\frac{t}{l}\right)\frac{\left(1+\frac{h}{l}\right)}{cos\theta\left(\frac{h}{l}+sin\theta\right)}$
G_{xy}	G_{xz}	G_{yz}
$\frac{E_m}{1-\nu_m{}^2}\frac{t^3(sin\theta+1)}{l^3cos\theta(6.25-9sin\theta)}$	$G_m\frac{2t}{lcos\theta(1+sin\theta)}$	$G_m\frac{10t}{9lcos^3\theta(1+sin\theta)}$
ν_{xy}	ν_{xz}	ν_{yz}
1.15	$\frac{\nu_m}{1-\nu_m{}^2}\frac{t^2(sin\theta+1)^2}{24l^2cos\theta\left(\frac{cos\theta}{3}-\frac{1+cos\theta}{8}\right)}$	$\frac{\nu_m}{1-\nu_m{}^2}\frac{t^2cos^2\theta}{2l^2sin^2\theta}$

Instead of treating the inclined walls solely as bending beams, Nast decomposes the unit cell into three regions, i.e. two inclined segments and a vertical segment representing the cell intersections. This modelling allows for a continuous deformation field across the entire cell, rather than isolated beam responses. Consequently, the model provides analytical expressions for in-plane Young modulus and shear moduli that inherently capture the full cell geometry. Nast model equations are reported in Table 2.

- **Shi & Tong homogenization model**

Shi & Tong propose a two-scale homogenization method [34] to derive the equivalent elastic moduli of honeycomb cores. The approach treats the honeycomb as a periodically heterogeneous medium and applies asymptotic expansions to solve the governing equations of elasticity across two spatial scales. Cell walls are modelled as beams capable of bending and stretching. Unlike the unit-cell-based averaging in classical models, this method introduces attempts to account for warping effects, periodicity, and local compliance, including junction flexibility. Analytical expressions for both in-plane and transverse shear moduli are obtained. Compared to Gibson & Ashby, which neglect through-thickness warping and provide lower-order estimates, the Shi & Tong formulation claims to be more accurate and physically consistent, especially in low-density or anisotropic configurations, by explicitly capturing the cell-level mechanics. Shi & Tong model equations are reported in Table 3.

- **Kumar homogenization model**

The Kumar model [35] is formulated on a strain-energy approach that employs Castigliano theorem to derive the effective orthotropic elastic constants of a periodic honeycomb core. Under in-plane loading, the derivation primarily considers the deformation of the inclined cell walls. The vertical walls contribute negligibly to the longitudinal deflection under uniaxial compressive stress, which simplifies the strain energy calculation to the axial and bending components of the inclined walls. Neglecting shear deformation in these walls, a valid assumption when the wall length is much greater than its thickness, the effective longitudinal Young modulus is obtained from the derivative of the total strain energy with respect to the applied load. Similar procedures yield the expressions for the in-plane transverse modulus, in-plane shear modulus, and the associated Poisson ratios. For the out-of-plane behaviour, the model extends the strain energy formulation to account for tensile and shear deformations when loads are applied perpendicular to the cell plane. A crucial assumption here is the neglect of certain higher-order shear effects, justified by the relative dimensions of the cell walls. Kumar model equations are reported in Table 4.

- **Sorohan homogenization model**

The analytical model proposed by Sorohan [36,37] is based on a refined homogenization approach for hexagonal honeycombs under axial and shear loading. In contrast to the classical Gibson & Ashby formulation, which treats the cell walls as beams undergoing bending and makes assumptions on the node geometry, this model introduces a generalized representation of the repetitive unit cell, incorporating equivalent parallelepipedal blocks for both inclined and vertical walls. The nodal regions, whose real geometry is highly variable, are also modelled as equivalent blocks, enabling the application of Timoshenko beam theory. Effective in-plane properties are derived using strain energy methods, taking into account bending, shear, and axial contributions. Correction factors introduced to account for plane strain effects and stress redistribution across the node surfaces. The model aims to improve accuracy for non-regular configurations, including commercial honeycombs with double vertical walls or re-entrant geometries. Sorohan model equations are reported in Table 5. It is worth pointing out that the Sorohan model has no predictive capability for the out-of-plane properties, and for the purpose of applying it to our study-cases, these properties were considered equal to those predicted by Kumar model.

where the coefficients k_1, k_2, k_{12}, c_{12}, are:

$$k_1 = \frac{1}{1+\left(\frac{t}{l}\right)^2(2.4+1.5\nu_m+\cot^2\theta)} \tag{1}$$

$$k_2 = \frac{1}{1+\left(\frac{t}{l}\right)^2(2.4+1.5\nu_m+\tan^2\theta+\frac{2h}{lcos^2\theta})} \tag{2}$$

$$k_{12} = \frac{1+\frac{2h}{l}}{1+\frac{2h}{l}+\left(\frac{t}{l}\right)^2\left[\left(\frac{l}{h}\right)(2.4+1.5\nu_m)\left(2+\frac{h}{l}+sin\theta\right)+\frac{\left(\frac{h}{l}+sin\theta\right)}{\left(\frac{h}{l}\right)^2}\left(\left(\frac{h}{l}+sin\theta\right)\tan^2\theta+sin\theta\right)\right]} \tag{3}$$

Table 3
Equivalent mechanical properties: Shi & Tong model.

E_x	E_y	E_z
$E_m\frac{\sqrt{3}}{5}\left(\frac{t}{h}\right)$	$E_m\frac{\sqrt{3}}{5}\left(\frac{t}{h}\right)$	$E_m\left(\frac{t}{l}\right)\frac{\left(1+\frac{h}{l}\right)}{cos\theta\left(\frac{h}{l}+sin\theta\right)}$
G_{xz}	G_{xz}	G_{yz}
$E_m\sqrt{3}\left(\frac{t}{h}\right)^3$	$G_m\frac{\sqrt{3}}{2}\left(\frac{t}{h}\right)$	$G_m\frac{1}{\sqrt{3}}\left(\frac{t}{h}\right)$
ν_{xy}	ν_{xz}	ν_{yz}
1	0	0

$$c_{12}=\frac{1+\left(\frac{t}{l}\right)^2(1.4+1.5\nu_m)}{1+\left(\frac{t}{l}\right)^2(2.4+1.5\nu_m+\cot^2\theta)} \tag{4}$$

2.2. Considerations on RVE-based homogenization strategies

Although this work focuses on analytical homogenization methods, it is worth noting that alternative strategies based on the concept of Representative Volume Elements (RVEs) [38,39] could provide a more general framework for the derivation of equivalent mechanical properties. In RVE-based approaches, the core mechanical response is evaluated by solving boundary problems defined on a sufficiently large and representative subdomain of the material [40,41]. Under prescribed loading conditions, the RVE macroscopic stress–strain response can be computed through numerical simulations, often using FEM simulations. This information is then used to compute the effective stiffness tensor, thus establishing the constitutive behaviour of the equivalent continuum, typically in the form of a generalized Hooke law. Hence, RVE approaches do not rely on idealized assumptions about cell shape or deformation mechanisms, and can naturally incorporate complex local effects such. However, they also require considerably more computational effort and could lack the closed-form transparency that makes analytical methods appealing for rapid parametric studies. In this respect, RVE-based strategies offer an important complement to the analytical formulations presented in this study and may serve as reference solutions for model calibration or validation in future developments.

2.3. Cuf-based beam models for sandwich structures

Carrera Unified Formulation offers a framework to formulate and solve structural problems using 1D, 2D, or 3D theories under a unified notation. Its core idea is to represent the kinematics of deformation through a hierarchical expansion of the displacement field using a set of generalized coordinates and polynomial shape functions. The fundamental advantage of CUF lies in its flexibility: by simply adjusting the expansion order and the number of cross-sectional layers or components, it becomes possible to recover Equivalent Single Layer (ESL), Layer-Wise (LW), or Component-Wise (CW) theories within a single mathematical structure. CUF formalism employs the concept of a fundamental nucleus, which defines the smallest computational entity from which all governing equations are assembled. The governing equations are automatically derived once the polynomial expansion functions and the interpolation scheme along the beam axis are defined. This approach allows for modelling 3D-like behaviour using 1D beam

Table 4
Equivalent mechanical properties: Kumar model.

E_x	E_y	E_z
$\frac{E_m\left(\frac{t}{l}\right)cos\theta}{\left(\frac{h}{l}+sin\theta\right)\left[cos^2\theta+\left(\frac{l}{t}\right)^2sin^2\theta\right]}$	$\frac{E_m\left(\frac{t}{l}\right)\left(\frac{h}{l}+sin\theta\right)}{cos\theta\left[sin^2\theta+\left(\frac{t}{l}\right)^2cos^2\theta\right]}$	$E_m\left(\frac{t}{l}\right)\frac{\left(1+\frac{h}{l}\right)}{cos\theta\left(\frac{h}{l}+sin\theta\right)}$
G_{xz}	G_{xz}	G_{yz}
$E_m\left(\frac{t}{l}\right)^3\left(\frac{l}{h}\right)^2\frac{\left(\frac{h}{l}+sin\theta\right)}{cos\theta\left(1+\frac{h}{4l}\right)}$	$G_m\left(\frac{t}{l}\right)\frac{cos\theta}{\left(\frac{h}{l}+sin\theta\right)}$	$G_m\left(\frac{t}{l}\right)\frac{\left(\frac{h}{l}+sin\theta\right)}{cos\theta\left(1+\frac{h}{l}\right)}$
ν_{xy}	ν_{xz}	ν_{yz}
$\frac{sin\theta\left[1+\left(\frac{l}{t}\right)^2\right]}{\left(\frac{h}{l}+sin\theta\right)\left[1+\left(\frac{l}{t}\right)^2tan^2\theta\right]}$	$\nu_m\frac{E_x}{E_z}$	$\nu_m\frac{E_y}{E_z}$

Table 5
Equivalent mechanical properties: Sorohan model.

E_x	E_y	E_z
$E_mk_1\left(\frac{t}{L}\right)^3\frac{cos\theta}{\left(\frac{h}{l}+sin\theta\right)sin^2\theta}$	$E_mk_2\left(\frac{t}{L}\right)^3\frac{\left(\frac{h}{l}+sin\theta\right)}{cos^3\theta}$	$E_m\left(\frac{t}{l}\right)\frac{\left(1+\frac{h}{l}\right)}{cos\theta\left(\frac{h}{l}+sin\theta\right)}$
G_{xy}	G_{xz}	G_{yz}
$E_mk_{12}\left(\frac{t}{L}\right)^3\frac{\left(\frac{h}{l}+sin\theta\right)}{\left(\frac{h}{l}\right)^2\left(2\frac{h}{l}+1\right)cos\theta}$	$G_m\left(\frac{t}{l}\right)\frac{cos\theta}{\left(\frac{h}{l}+sin\theta\right)}$	$G_m\left(\frac{t}{l}\right)\frac{\left(\frac{h}{l}+sin\theta\right)}{cos\theta\left(1+\frac{h}{l}\right)}$
ν_{xy}	ν_{xz}	ν_{yz}
$c_{12}\frac{cos^2\theta}{\left(\frac{h}{l}+sin\theta\right)sin\theta}$	$\nu_m\frac{E_x}{E_z}$	$\nu_m\frac{E_y}{E_z}$

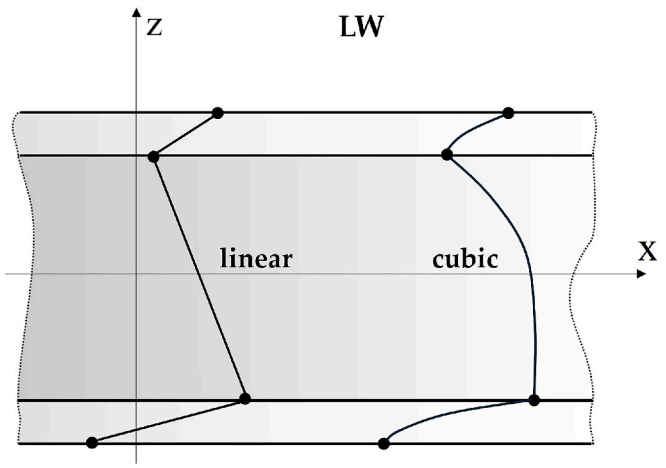


Fig. 2. LW qualitative representation of displacement field (linear and cubic): image adapted form ref. [27].

elements, where the beam axis can be arbitrarily oriented within the structure depending on the modelling needs.

2.4. Layer-Wise modelling

The Layer-Wise theory assigns independent displacement variables to each individual layer of the structure. Within this framework, the mechanical properties are homogenized by treating each layer separately. According to the LW approach, the displacement fields are defined as:

$$\boldsymbol{u}^{\boldsymbol{k}} = F_\tau \, \boldsymbol{u}^{\boldsymbol{k}}_\tau, \qquad \tau = 1, 2, \cdots, N \tag{5}$$

Where k is the number of layers and F_τ are expansion functions, Lagrange polynomials in this case, defined at the k-layer level. In the LW approach, the problem can be posed as a general N-order Lagrange polynomial, by adding higher-order terms, as:

$$\begin{aligned} u^k_x(x,y,z) &= F_1(x,z)u^k_{x1}(y) + F_2(x,z)u^k_{x2}(y) + \ldots + F_N(x,z)u^k_{xN}(y) \\ u^k_y(x,y,z) &= F_1(x,z)u^k_{y1}(y) + F_2(x,z)u^k_{y2}(y) + \ldots + F_N(x,z)u^k_{yN}(y) \\ u^k_z(x,y,z) &= F_1(x,z)u^k_{z1}(y) + F_2(x,z)u^k_{z2}(y) + \ldots + F_N(x,z)u^k_{zN}(y) \end{aligned} \tag{6}$$

The LW theory enables the modeling of local phenomena occurring within individual layers. A qualitative representation of the displacement field in a multilayered structure is shown in Fig. 2. While this approach can capture such local effects, it demands computational resources that scale with the number of layers. In LW-based models, the mechanical properties must be homogenized at the layer level. The assembled model built according to CUF-based LW representation, is schematically reported in Fig. 3.

2.5. Component-Wise modelling

Component-Wise theories achieve the highest level of modeling detail by treating each structural part, such as the skins and the core in a sandwich structure, as separate subdomains. As a result, there is no need for structural homogenization or simplifications, the actual geometry can be represented, together with the layers interface. This method is especially effective in representing complex interactions between components with significantly different mechanical behaviors, for example anisotropic cores coupled with stiff face sheets. In CW models, multilayered structures can be represented without any need for property homogenization or geometrical simplifications, allowing for an accurate depiction of the real structural layout. In this formulation, the sandwich panel is modeled using 1D beam elements, with the beam axis oriented along the height direction of the sandwich, as illustrated in Fig. 4.

In CW formulation, the cross-sections of both the skins and the honeycomb core are discretized using high-order Lagrange polynomials. Similar to LW approach, the displacement field can still be described as

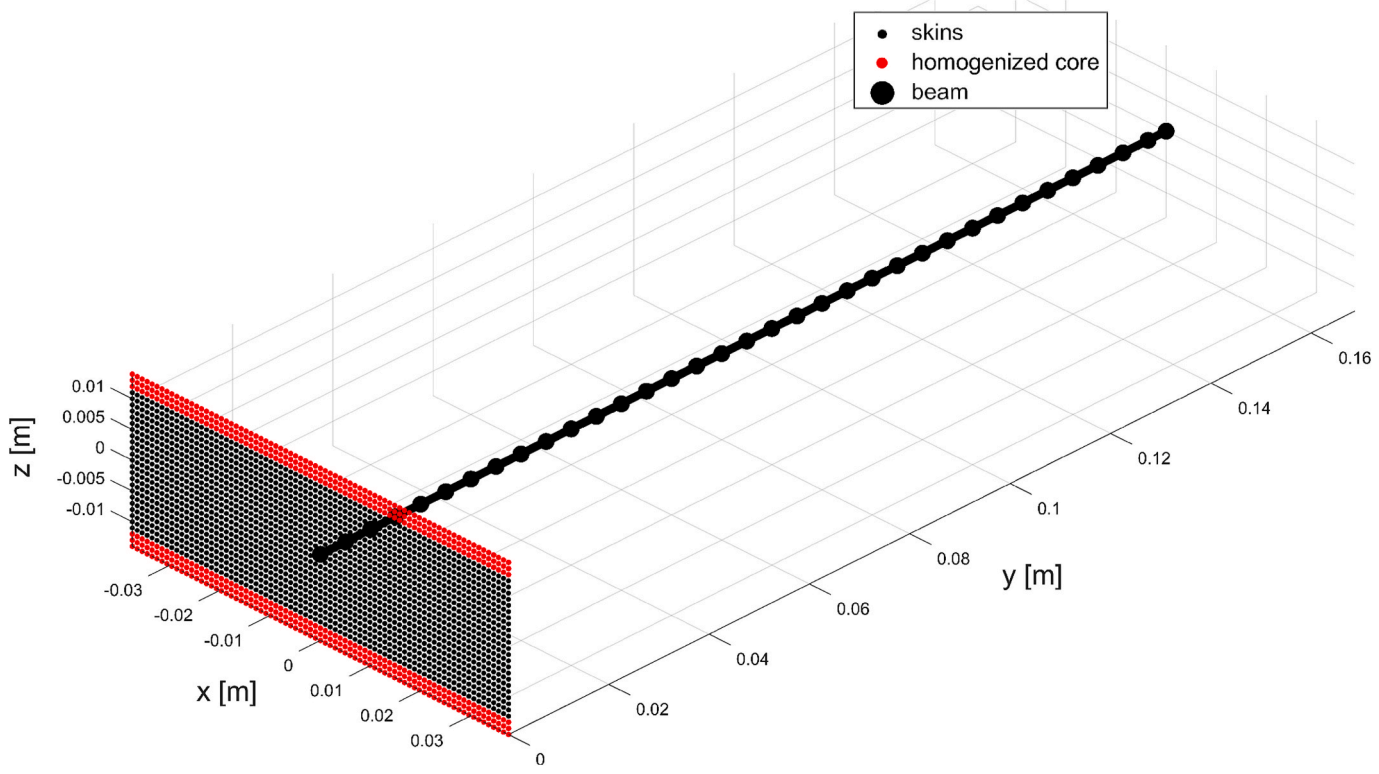


Fig. 3. Scheme of a CUF-based LW model of a sandwich structure.

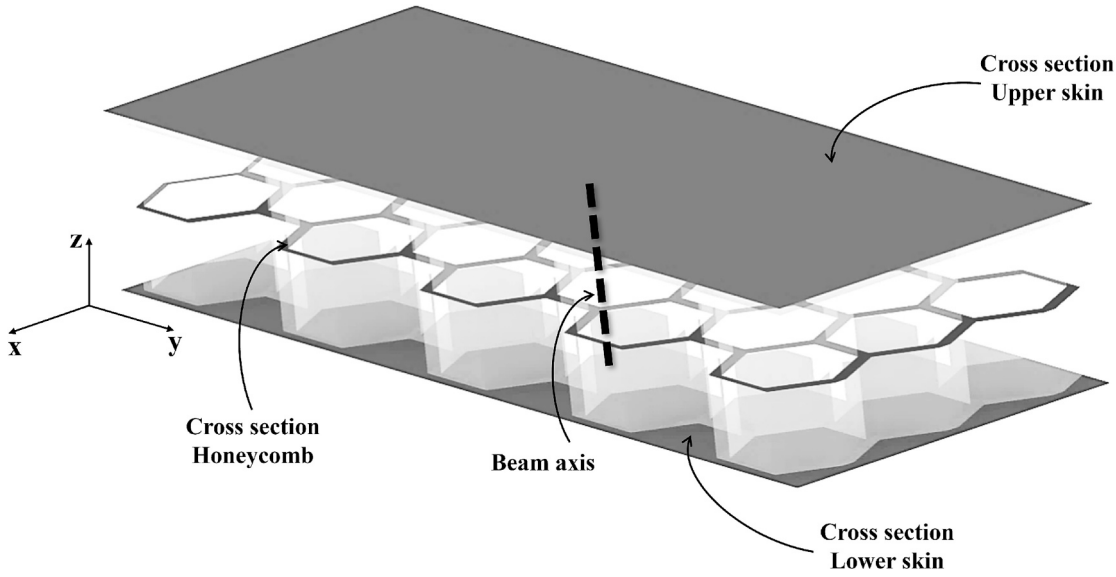


Fig. 4. Scheme of the CW modelling of the sandwich structure.

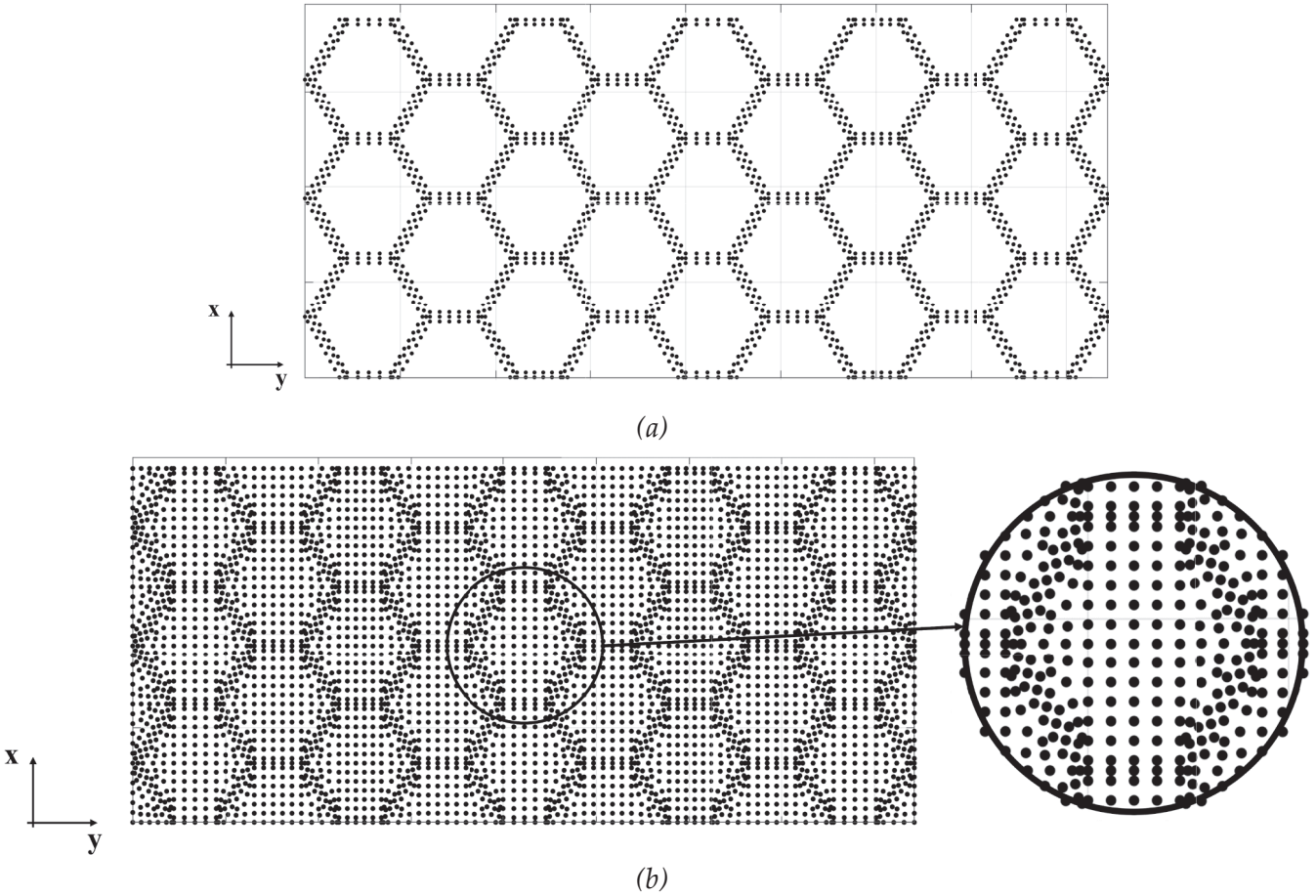


Fig. 5. Lagrangian cross-section discretization of: (a) honeycomb; (b) skin.

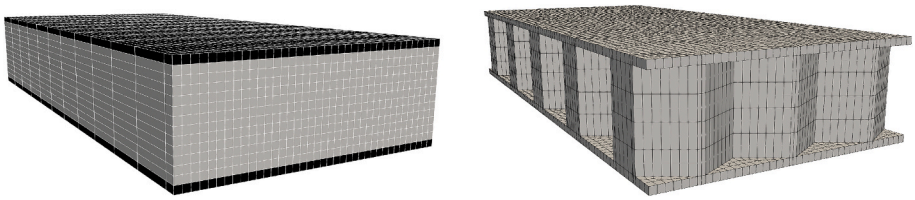


Fig. 6. LW (left) and CW (right) sandwich representation.

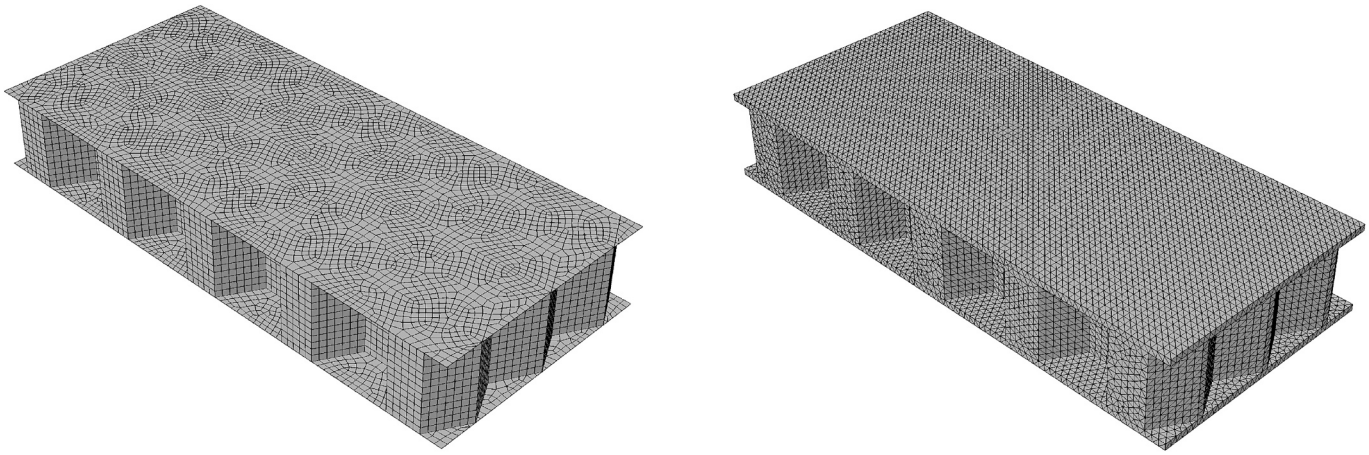


Fig. 7. Sandwich FE models: 2D (left) and 3D (right).

Table 6
Sizes of the mesh for the FEM and CUF modelling approaches.

	Mesh seed	n° elements	n° nodes	DoFs
Mesh 2D	2 mm	14,833	14,218	**85,308**
Mesh 3D	2 mm	125,169	220,988	**662,964**
CUF	–			**113,604**

in Eq. (6); however, in this case, the index k refers to the k-th structural component. A distinctive aspect of this CW modeling approach concerns the definition of the sandwich cross-section and the orientation of the corresponding beam axis. Consequently, the displacement field, represented through N-order Lagrange expansions, is reformulated as follows:

$$\begin{aligned} u_x(x,y,z) &= F_1(x,y)u_{x1}(z) + F_2(x,y)u_{x2}(z) + \ldots + F_N(x,y)u_{xN}(z) \\ u_y(x,y,z) &= F_1(x,y)u_{y1}(z) + F_2(x,y)u_{y2}(z) + \ldots + F_N(x,y)u_{yN}(z) \\ u_z(x,y,z) &= F_1(x,y)u_{z1}(z) + F_2(x,y)u_{z2}(z) + \ldots + F_N(x,y)u_{zN}(z) \end{aligned} \tag{7}$$

The expansion functions for the cross-section are defined in the x-y plane, as shown in Fig. 5, while the beam axis is aligned with the z-direction, corresponding to the sandwich thickness, see Fig. 4. To enforce displacement continuity at the interfaces between components, shared Lagrange nodes are introduced. This strategy guarantees compatibility of both displacements and strains between the face sheets and the honeycomb core, ensuring interface continuity. The mesh of the skins must include these common nodes to avoid discontinuities. A precise alignment of the shared Lagrange points enables effective coupling between core and skins, as illustrated in Fig. 5, ensuring an accurate representation of the interface behavior.

The displacement field is then described along the beam axis by means of Finite Element approximation, as in Eq. (8):

$$\boldsymbol{u}_\tau(y) = N_i(y)\boldsymbol{q}_{\tau i} i = 1, 2, \cdots N \tag{8}$$

N_i are the shape functions for the beam axis representation, and $\boldsymbol{q}_{\tau i}$ are nodal unknowns. By incorporating this approximation into the complete expression of the displacement field, the corresponding virtual variation of the field becomes:

$$\delta\boldsymbol{u}(x,y,z) = F_s(x,z)N_j(y)\delta\boldsymbol{u}_{js} s = 1, 2, \cdots, Mj = 1, 2, \cdots N \tag{9}$$

The representations of the LW and CW modelling of a honeycomb sandwich are reported in Fig. 6.

2.5.1. Comparison with FEM models

Several validation studies of the Carrera Unified Formulation (CUF) have already appeared in the literature, based on comparisons with either high-fidelity numerical benchmarks or experimental data. As a representative example, here the investigation and outcomes of the recent study of ref. [30] are reported. In this reference, are systematically assessed the mechanical response of sandwich panels subjected to various static loading conditions. A benchmark sandwich panel was analysed: after a mesh-convergence study, the 2D FEM model (Fig. 7-left), the 3D FEM model (Fig. 7-right) and the CUF CW model required the numbers of degrees of freedom listed in Table 6. The CUF CW solution reached an accuracy essentially equal to that of the 3D FEM model while demanding only one-sixth of the degrees of freedom. Moreover, the CUF CW approach can capture the through-thickness stress field, local stress peaks at concentration zones and the full three-dimensional strain distribution throughout the core, capabilities that the less expensive 2D FEM model, by definition, cannot offer.

3. Study cases

This section provides a description of the reference study cases used in this work to assess the accuracy of homogenized models for sandwich honeycomb cores. To assess the impact of geometrical configuration on the accuracy of analytical models, two distinct cellular architectures are investigated. These configurations differ not only in scale, but also in regularity and aspect ratio, offering a broad testbed to examine the robustness and limitations of the selected equivalent-property models. The first configuration corresponds to a regular hexagonal cell, see Fig. 8-left, representing a canonical geometry commonly found in theoretical and commercial honeycomb cores. The second configuration

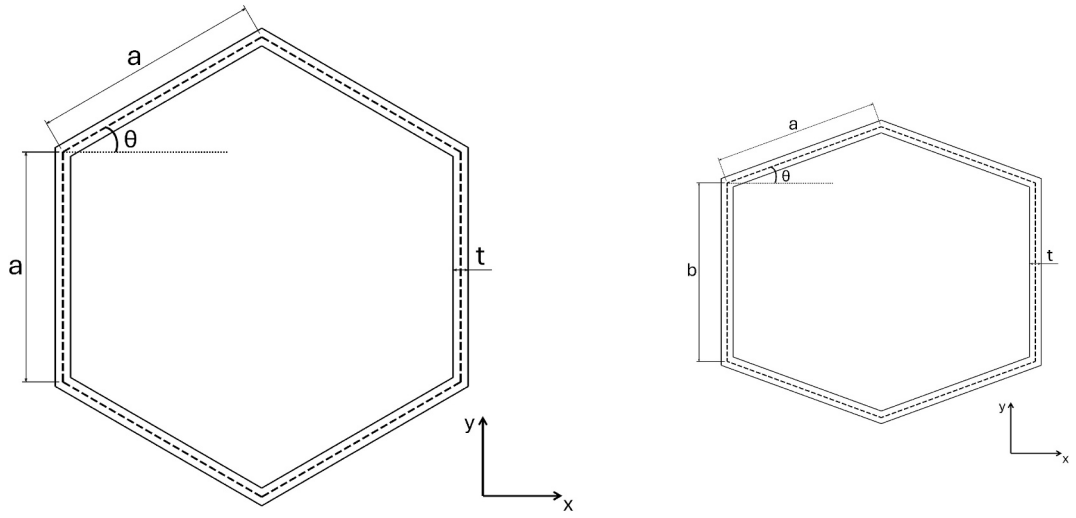


Fig. 8. Selected RCE: regular cell (left), non-regular cell (right).

is a non-regular hexagonal cell, deliberately selected to introduce geometrical irregularity and reduced size. In this case, the internal angle is reduced, and the cell edges are shortened, resulting in a smaller and more compact topology. Furthermore, the wall thickness is halved compared to the regular cell, thereby decreasing the relative density and altering the cell stiffness-to-mass ratio significantly. The geometrical features of the two selected RCE are reported in Table 7. These choices aim to simulate two different design philosophies, trying to identify possible limitations of the homogenization models directly related to the geometrical choices related to the RCE.

For the same reason, also the sandwich layout is differentiated between the two configurations, as illustrated in Fig. 9 and Fig. 10. The regular-cell configuration occupies a wider and longer domain, while the non-regular configuration is smaller but with a higher aspect ratio. The dimensions of the sandwich planforms are reported in Table 8.

In both cases, the sandwich consists of two isotropic aluminium skins and a central core, also made by aluminium. To assess the influence of the core thickness, three distinct sandwich height values are examined: h_1=10 mm h_2=20 mm, andh_3 = 40 mm, as sketched in Fig. 11.

The test cases have been specifically designed to expose the sensitivity of homogenization models to a set of geometric features that are known to influence the mechanical behaviour of the sandwich structure. The variation in cell size, with a characteristic length almost halved in the non-regular configuration, introduces clear scale effects. At the same time, the wall thickness is also reduced by a factor of two in the non-regular case, resulting in a lower relative density and a significant reduction in local stiffness. Additionally, deviating from a 30° internal angle affects the regularity of the cells geometry. This geometric differentiation is further intensified by changes in beam overall size and aspect ratio. Lastly, a difference in honeycomb arrangement is introduced: while the non-regular panel terminates with a full row of complete hexagonal cells, the regular core features a truncated final row, hence exhibiting a different edge condition.

For both configurations, the full set of orthotropic elastic constants have been computed using the different analytical model described in Section 2. The resulting equivalent properties for the regular and non-regular honeycomb configurations are summarized in Table 9 and Table 10. While a detailed comparative discussion is deferred to the next section, it is worth noting that the observed values differ significantly across both geometry and model. Notably, Shi-Tong model seems to largely overestimate the in plane moduli E_x, E_y. For the other models, in-plane Young moduli and shear modulus G_{xy} exhibit variation, particularly in the non-regular configuration. Out-of-plane Young modulus is assessed in the same way for all the different models.

Table 7
Geometric features of the two selected RCE.

	Regular cell	Non-regular cell
a [mm]	30	15
b [mm]	–	13.8
θ [deg]	30	20
t [mm]	2	1

4. Results

4.1. Linear-static analysis: Bending

The linear-static bending analysis is performed by applying a concentrated vertical load F = 2500 N at the free end of the sandwich panel, while the opposite end is fully clamped, preventing both translational and rotational motion, as sketched in Fig. 12.

In the bending tests under tip-loading with the fixed root section, the maximum vertical displacement $u_{z\,max}$ serves as a robust indicator of the global stiffness. The analysis reveals significant differences in predictive behaviour among the various homogenization models, and these differences correlate closely with the underlying equivalent mechanical properties derived from the analytical formulations.

For the regular honeycomb cell configuration, the results are reported in Table 11. In this context, the Gibson, Nast, Kumar, and Sorohan models produce effective stiffnesses that, while having the same formulation for the out-of-plane modulus E_z, exhibit some differences in the in-plane moduli (E_x, E_y) and the shear moduli (G_{xy}, G_{xz}). These differences translate into distinct predictions of deflection. The models yielding lower in-plane moduli (e.g. Gibson approach) tend to produce an overestimation of $u_{z\,max}$ when compared to the high-fidelity CW model. This overestimation significantly increases with the height of the sandwich structure. Conversely, the Shi-Tong model, which assumes higher in-plane stiffness, with notably high E_x and E_y values, consistently underestimates $u_{z\,max}$. This behaviour is particularly pronounced at lower structural heights, where the role of the core properties is amplified. The key technical insight is that the homogenization procedure does not adjust for the effective bending stiffness of the sandwich assembly in a way that fully captures the layered interactions, especially as the geometry deviates from the idealized assumptions used in the derivations. As the cell regularity offers a symmetric and predictable load path, the discrepancies can be directly linked to the sensitivity of the analytical models to the in-plane moduli and shear couplings.

In the irregular cell configuration, the differences are even more

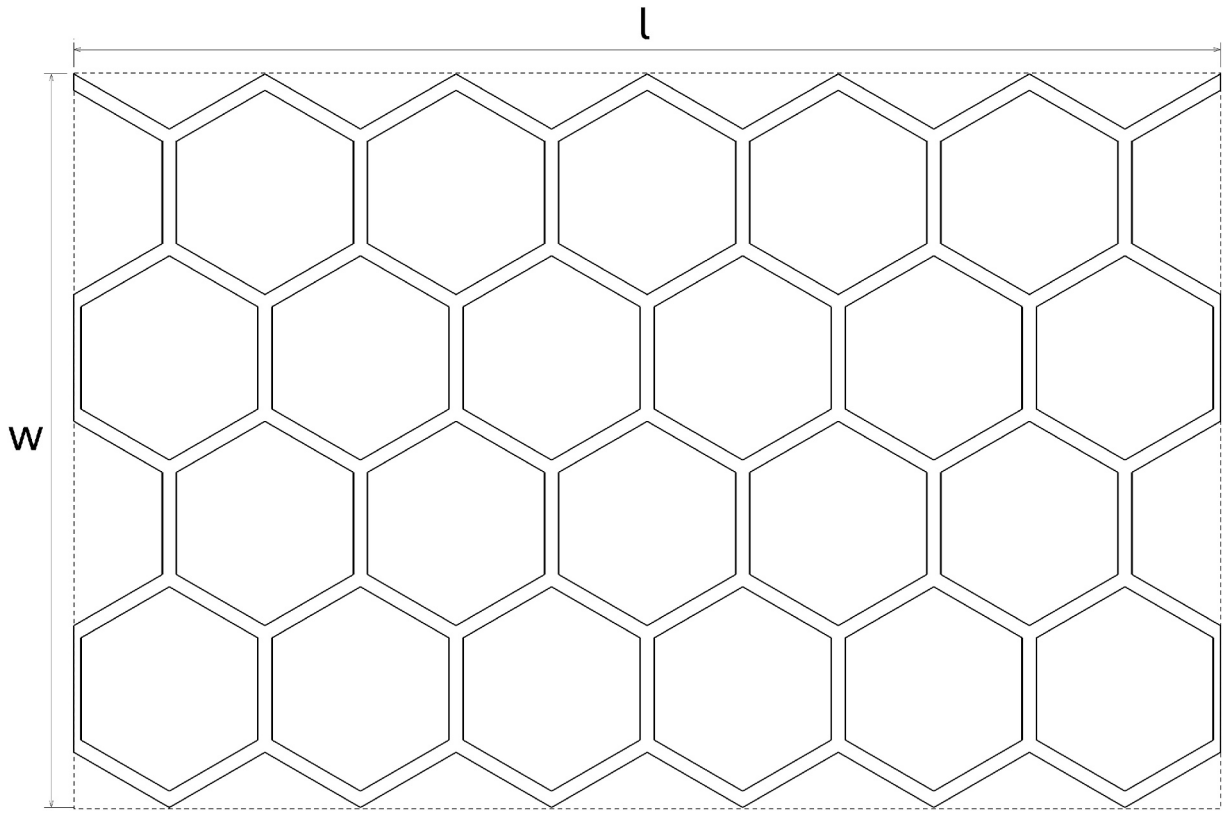


Fig. 9. Arrangement and size of honeycomb core with regular cells.

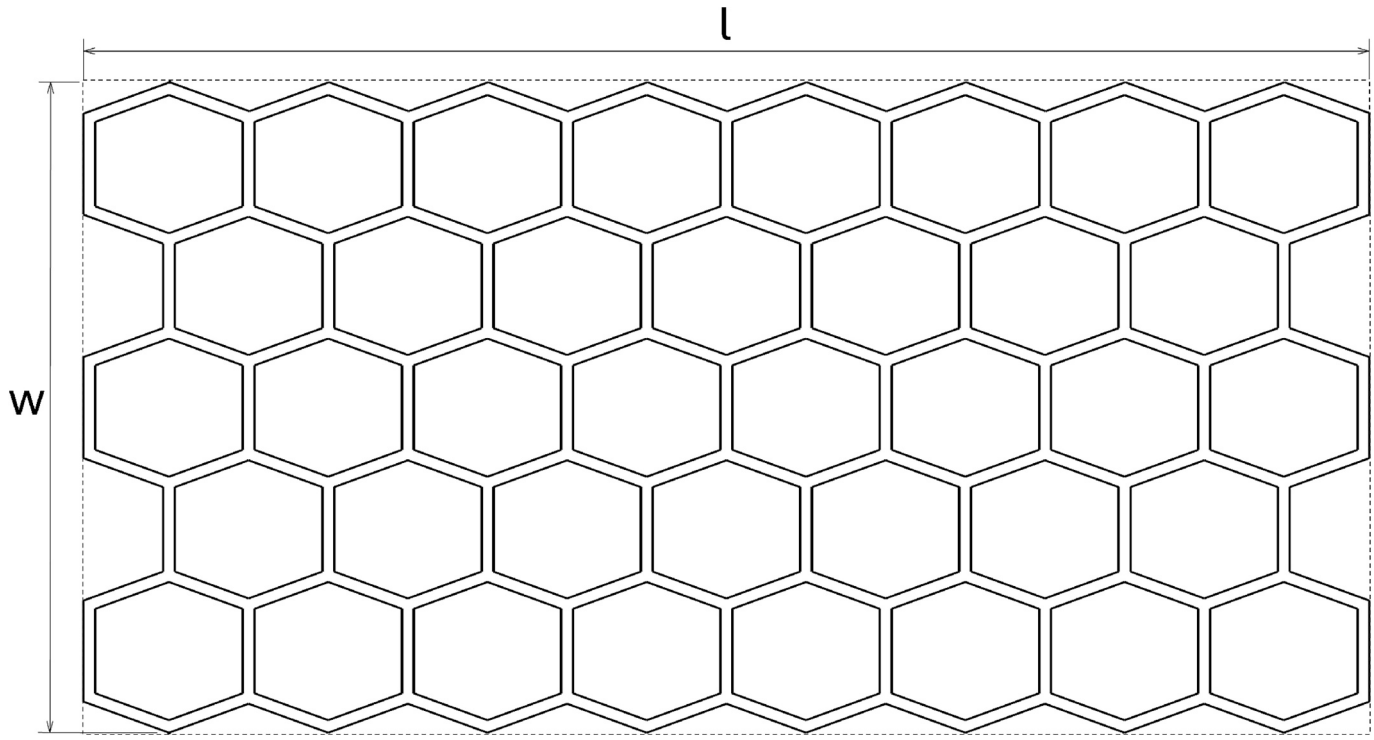


Fig. 10. Arrangement and size of honeycomb core with non-regular cells.

pronounced, as reported in Table 12. The RCE, characterized by irregularity of the hexagon, reduced dimensions and a lower wall thickness, leads to a different set of equivalent properties with respect to that of the regular honeycomb case. Examining the displacement results for the irregular case with a skin thickness of 1 mm, the high-fidelity CW model records maximum deflections that are modest relative to the regular case; this depend from both cell and structure geometry. Here, the Gibson model, shows an underestimation of deflection, whereas the

Table 8
Sandwich main dimensions.

	Regular cell honeycomb	Non-regular cell honeycomb
l [mm]	324 mm	218 mm
w [mm]	207 mm	110 mm

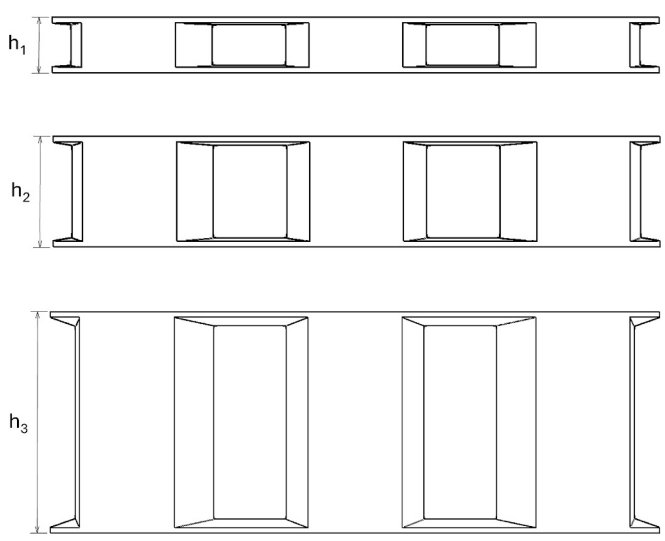


Fig. 11. Different sandwich heights.

Nast, Kumar, and Sorohan models result in a significant overestimation of $u_{z\ max}$. This highlights that slight differences in the equivalent properties could shift the predictions from conservative to not conservative Table 13 and Table 14.

The key factor here appears to be the G_{xy}, that exhibits lower values in the Nast and Sorohan formulations, and to a lesser extent in the Kumar model; this reduces the effective coupling between the skins and core during bending. In other words, low shear stiffness reduces the capability of the sandwich core to efficiently transfer forces to the outer skins. Even though Nast higher E_x might suggest a stiffer response, the concurrent reduction in shear stiffness undermines the overall flexural rigidity, leading to an overestimation of $u_{z\ max}$. While the effective shear moduli and in-plane stiffnesses primarily govern the bending response of the sandwich structure, the Poisson ratios may also exert an influence, but their effect is generally of secondary order in this context. Variations in ν primarily affect the lateral contraction and minor coupling terms between orthogonal directions, but they do not directly enter the leading-order expressions for the bending rigidity. In the irregular cell case, although models such as Gibson, Nast, Kumar, and Sorohan exhibit notable differences in their computed ν_{xy} these differences have a relatively smaller impact on the deflection response when compared to the disparities in shear modulus and in-plane moduli.

The variation of the overall sandwich height offers further insight into the interplay between the homogenized properties and global structural behaviour. With increasing *h*, the sandwich beam exhibits lower absolute displacements due to an increase in bending stiffness. However, the relative error between the LW and CW models tends to grow. This can be explained by the fact that the homogenization models derive equivalent properties independent of *h*, while the actual stiffness of a layered assembly is significantly affected by the beam height. Hence, the effect of a higher *h* amplifies the discrepancies: the distance

Table 9
Equivalent mechanical properties for the regular honeycomb core.

Model	E_x [MPa]	E_y [MPa]	E_z [MPa]	G_{xy} [MPa]	G_{xz} [MPa]	G_{yz} [MPa]	ν_{xy}	ν_{xz}	ν_{yz}
Gibson	51.3	51.3	8977	32.1	1001	1501	1	$2.2x10^{-3}$	$2.2x10^{-3}$
Nast	57.6	74.9	8977	24.7	2668	1976	1.15	$3.2x10^{-3}$	$2.4x10^{-3}$
Shi-Tong	1732	1732	8977	38.5	1001	1501	1	0	0
Sorohan	50.0	50.0	8977	12.8	1001	1501	0.98	$2.1x10^{-3}$	$2.1x10^{-3}$
Kumar	50.6	51.2	8977	30.8	1001	1501	1	$2.1x10^{-3}$	$2.1x10^{-3}$

Table 10
Equivalent mechanical properties for the non-regular honeycomb core.

Model	E_x [MPa]	E_y [MPa]	E_z [MPa]	G_{xy} [MPa]	G_{xz} [MPa]	G_{yz} [MPa]	ν_{xy}	ν_{xz}	ν_{yz}
Gibson	160.4	49.2	11,504	45.6	1239.1	1372.8	1.81	$6.2x10^{-3}$	$1.9x10^{-3}$
Nast	191.7	57.3	11,504	14.4	2988.0	1879.9	1.15	$2.2x10^{-3}$	$7.3x10^{-3}$
Sorohan	152.1	47.8	11,504	11.56	1239.1	1372.8	1.73	$6.0x10^{-3}$	$1.9x10^{-3}$
Kumar	154.3	49.1	11,504	28.9	1239.1	1372.8	0.55	$6.0x10^{-3}$	$1.9x10^{-3}$

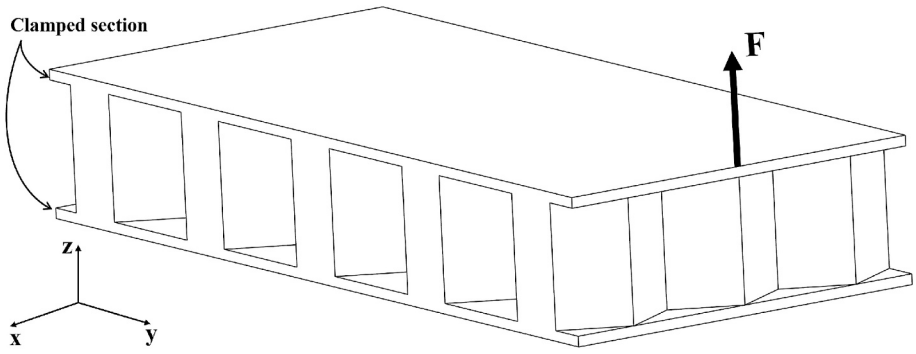


Fig. 12. Scheme of the bending loading condition.

Table 11
Results in terms of maximum vertical displacement for the regular honeycomb structure.

		CW	Gibson	Nast	Shi-Tong	Kumar	Sorohan
h = 10 mm	$u_{z\,max}$ **[mm]**	39.7	42.9	43.3	16.6	41.6	43.2
	Δ%$u_{z\,max}$	ref.	+8.1	+9.1	−58.2	+4.8	+8.8
h = 20 mm	$u_{z\,max}$ **[mm]**	8.6	9.7	9.9	4.4	9.1	9.8
	Δ%$u_{z\,max}$	ref.	+12.8	+15.1	−48.8	+5.8	+14.0
h = 40 mm	$u_{z\,max}$ **[mm]**	1.9	2.4	2.5	1.3	2.2	2.4
	Δ%$u_{z\,max}$	ref.	+26.3	+31.6	−31.6	+15.8	+26.3

Table 12
Results in terms of maximum vertical displacement for the non-regular honeycomb structure.

		CW	Gibson	Nast	Kumar	Sorohan
h = 10 mm	$u_{z\,max}$ **[mm]**	22.6	20.9	25.2	25.4	24.8
	Δ%$u_{z\,max}$	ref.	−7.5	+11.5	+12.4	+9.7
h = 20 mm	$u_{z\,max}$ **[mm]**	4.8	4.2	5.9	6.0	5.7
	Δ%$u_{z\,max}$	ref.	−12.5	+22.9	+25.0	+18.8
h = 40 mm	$u_{z\,max}$ **[mm]**	1.1	1.0	1.6	1.7	1.6
	Δ%$u_{z\,max}$	ref.	−9.1	+45.5	+54.5	+45.5

Table 13
Results in terms of maximum vertical displacement for the non-regular honeycomb ($t_s = 0.2$ mm).

		CW	Gibson	Nast	Kumar	Sorohan
h = 10 mm	$u_{z\,max}$ **[mm]**	64.0	48.3	102.5	103.6	89.3
	Δ%$u_{z\,max}$	ref.	−24.5	+60.2	+61.9	+39.5
h = 20 mm	$u_{z\,max}$ **[mm]**	12.5	9.6	24.6	25.4	19.5
	Δ%$u_{z\,max}$	ref.	–23.2	+96.8	+103.2	+56.0
h = 40 mm	$u_{z\,max}$ **[mm]**	2.4	2.3	6.1	6.5	4.4
	Δ%$u_{z\,max}$	ref.	−4.2	+154.2	+170.8	+83.3

Table 14
Results in terms of maximum vertical displacement for the non-regular honeycomb ($t_s = 2$ mm).

		CW	Gibson	Nast	Kumar	Sorohan
h = 10 mm	$u_{z\,max}$ **[mm]**	15.5	14.9	15.7	15.9	15.8
	Δ%$u_{z\,max}$	ref.	−3.9	+1.3	+2.6	+1.9
h = 20 mm	$u_{z\,max}$ **[mm]**	2.9	2.9	3.3	3.4	3.4
	Δ%$u_{z\,max}$	ref.	=	+13.8	+17.2	+17.2
h = 40 mm	$u_{z\,max}$ **[mm]**	0.7	0.7	0.9	0.9	0.9
	Δ%$u_{z\,max}$	ref.	=	+28.6	+28.6	+28.6

between the skins and the neutral axis becomes larger, making inaccuracies in the in-plane and shear stiffness estimations more critical for the overall bending response. The regular cell configuration demonstrates a more gradual change in relative error with height, likely due to a more consistent load-sharing mechanism, whereas the irregular configuration exhibits sharper trends that underscore the combined effect of non-ideal geometry and height variation on the effective bending stiffness. These insights emphasize the importance of capturing the coupled effects in the derivation of equivalent properties, especially when the core geometry deviates from the regular ideal shape. The observed trend indicates that as the core geometry departs from regularity, the assumptions underlying some homogenization models could become less valid, leading to amplified errors in mechanical response prediction. The absence of the Shi-Tong model in this configuration, due to its inapplicability to the irregular geometry, further highlights the sensitivity of the analytical homogenization methods to geometric regularity.

For the irregular case, additional analyses were performed by varying the skin thickness, which directly influences the composite bending stiffness. This investigation is relevant because the analytical homogenization models here discussed show no correlation with the skin thickness, which could instead play a relevant role in the structure mechanical response. Two different cases, with respect to the reference case of$t_s = 1$ mm, were analysed: one with reduced thickness$t_s = 0.2$ mm and one with increased thickness$t_s = 2$ mm. A thinner skin, t_s=0.2 mm, results in significantly higher deflections as the core becomes the dominant contributor to the global mechanical behaviour. Under these conditions, the inaccuracies in the equivalent properties are exacerbated, leading to more pronounced overestimations. This sensitivity highlights that when the skin is thin, even minor deviations in the computed core properties lead to significant differences in the overall stiffness. Conversely, when the skin is thickened, t_s=2 mm, its stiffness dominates the bending response. Under these circumstances, all homogenization models converge more closely to the CW results because the influence of the core equivalent properties is effectively mitigated by the skin increased contribution. Also in these cases, the effect of sandwich height *h* is evident. The Gibson model appears to benefit from the combined effect of the two geometrical parameters, with better accuracies for high *h*; however, the overall frame seems to discourage the conclusion that this model is generally accurate with such precision in describing this structural problem.

These results underscore that a robust and reliable application of homogenization theories in the analysis of sandwich structures demands careful consideration of both the inherent geometric features of the core and the overall structural layout. The ability to correlate the predicted equivalent properties with the actual mechanical response, as evidenced by the trends in $u_{z\,max}$, is essential for improving the accuracy of simplified layer-wise models in engineering practice. General conclusions are difficult to be derived, as the dependencies for the specific case could introduce significant variations to the accuracy of the simplified models.

4.2. Linear-static analysis: Torsion

The second loading condition considered, depicted in Fig. 13, corresponds to a pure torsion, where equal and opposite vertical forces are applied at the free end (one on the upper and one on the lower skin), while the opposite end of the panel is fully clamped.

This study case is performed to highlight a key limitation of homogenized in this context: the loss of predictive accuracy when the geometric and/or loading symmetry is broken. This is specifically the case considered here. The selected structure for these computations is the sandwich with regular cell honeycomb core, that features a pattern

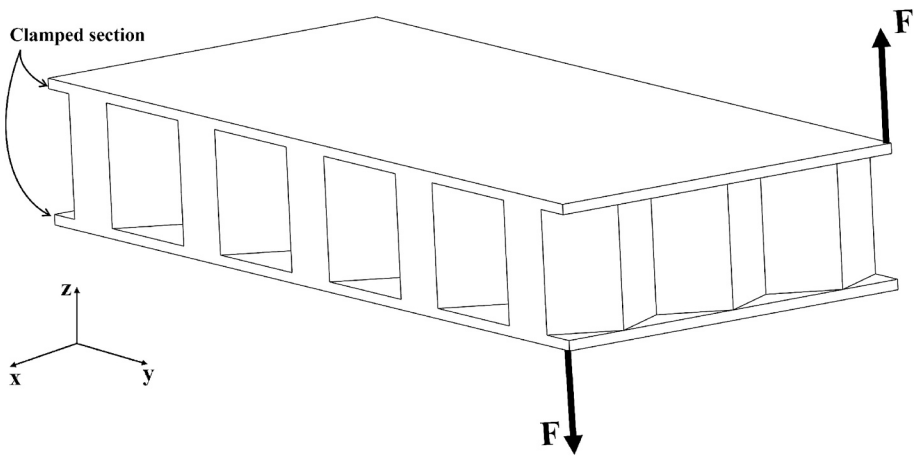


Fig. 13. Scheme of the torsion loading condition.

Table 15
Results in terms of maximum vertical displacement for the regular honeycomb structure.

		CW		LW-Kumar	
		right edge	**left edge**	**right edge**	**left edge**
h = 10 mm	$\lvert u_{z\,max}\rvert$ **[mm]**	24.1	16.6	18.1	18.1
	Δ%$\lvert u_{z\,max}\rvert$	ref.		−24.9	+9.0
h = 20 mm	$\lvert u_{z\,max}\rvert$ **[mm]**	11.6	3.8	4.7	4.7
	Δ%$\lvert u_{z\,max}\rvert$	ref.		−59.5	+23.7
h = 40 mm	$\lvert u_{z\,max}\rvert$ **[mm]**	8.9	0.9	1.6	1.6
	Δ%$\lvert u_{z\,max}\rvert$	ref.		−82.0	+77.8

of hexagonal cells not symmetric across the panel width, as represented in Fig. 9. The right and left sides of the core do not conclude in the same way: one edge ends with a full cell, the other with a halved cell.

In a CW model, which preserves the actual geometry of the complex sandwich structure, the mechanical property is actually represented according to the real physical case. The two vertical forces of torque are applied at points with different local stiffnesses: one force acts on a region directly supported by a cell, while the other is located above an unsupported edge. As a result, the mechanical response becomes inherently asymmetric. The stiffness mismatch between the two load application points generates a non uniformity in the torsional field response, which a homogenized LW model, by construction, cannot replicate. This example reveals a fundamental limitation of LW models: they assume that the core behaves as a layered orthotropic solid with continuous distribution of stiffness. Such a formulation cannot account for localized differences introduced by geometric discontinuities or loading asymmetry. To focus on this specific limitation, the proposed study-case comparison is restricted to a single reference homogenization model, i.e. Kumar, casually selected among those previously discussed. The results of the CW and LW simulations are summarized in Table 15. The values reported confirm the impact of geometric description. For example, $h = 10$ mm, the CW model predicts a vertical displacement at the right edge of 24.1 mm and 16.6 mm at the left edge, highlighting the asymmetry. The Kumar model, which distributes stiffness uniformly, predicts symmetric displacements of 18.1 mm on both sides, thus failing to capture the unbalanced response. As thickness increases, the asymmetry becomes more pronounced in CW, while the LW prediction remains symmetric by design.

These trends are further clarified by the vertical displacement contour maps shown in Fig. 14 and Fig. 15, for the CW and LW model respectively; as an example case, the structure featuring $h = 20$ mm is considered. The CW model displays a visible twist deformation with a steeper gradient localized near the right edge, where the skin is unsupported. The LW model, conversely, shows a regular and symmetric

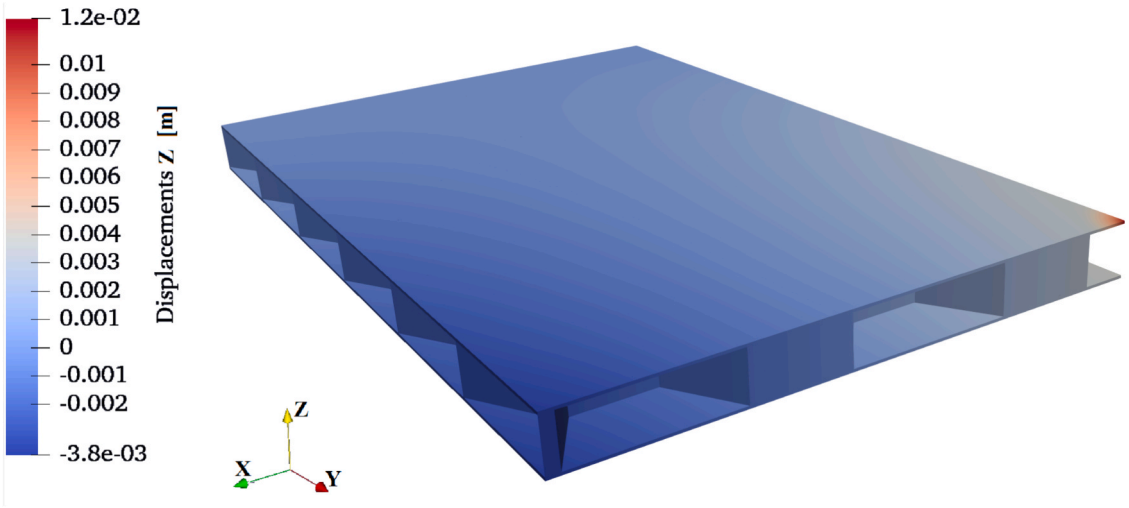


Fig. 14. Vertical displacement contour map, CW model, regular cell, $h = 20$ mm.

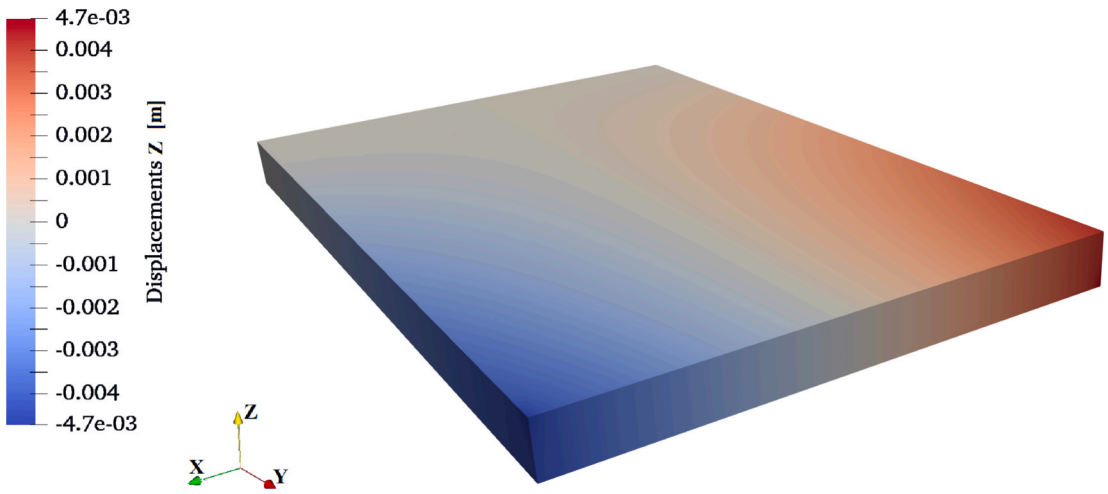


Fig. 15. Vertical displacement contour map, LW model, regular cell, $h = 20$ mm.

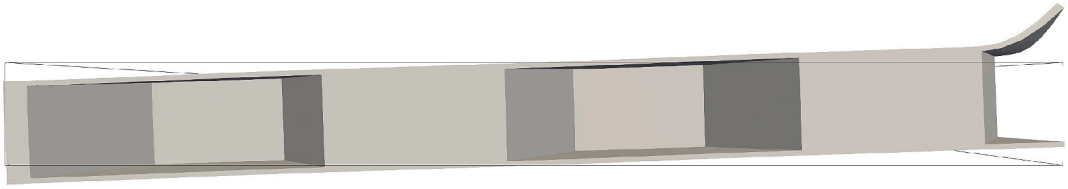


Fig. 16. Front view of the deformed shape, CW model, regular cell, $h = 20$ mm.



Fig. 17. Front view of the deformed shape, LW model, regular cell, $h = 20$ mm.

Table 16
First eight natural frequencies. Case: regular honeycomb, $h = 10$ mm, t_s=1 mm.

	CW	Gibson	Nast	Shi-Tong	Kumar	Sorohan
	f [kHz]					
Mode 1	0.107	0.108	0.107	0.191	0.110	0.108
Mode 2	0.342	0.345	0.355	0.355	0.352	0.351
Mode 3	0.635	0.644	0.654	1.030	0.663	0.651
Mode 4	1.102	1.119	1.101	1.855	1.141	1.110
Mode 5	1.175	1.128	1.175	2.055	1.157	1.150
Mode 6	1.566	1.635	1.692	2.271	1.679	1.659
Mode 7	1.723	1.811	1.869	3.490	1.880	1.835
Mode 8	2.107	2.184	2.321	3.939	2.272	2.251

Table 17
Natural frequencies percent difference. Case: regular honeycomb, $h = 10$ mm, t_s=1 mm.

	CW	Gibson	Nast	Shi-Tong	Kumar	Sorohan
			Δ%f (w.r.t. CW)			
	ref.					
Mode 1		+0.9	=	+78.5	+2.8	+0.9
Mode 2		+0.9	+3.8	+3.8	+2.9	+2.6
Mode 3		+1.4	+3.0	+62.2	+4.4	+2.5
Mode 4		+1.5	−0.1	+68.3	+3.5	+0.7
Mode 5		−4.0	=	+74.9	−1.5	−2.1
Mode 6		+4.4	+8.0	+45.0	+7.2	+5.9
Mode 7		+5.1	+8.5	+102.6	+9.1	+6.5
Mode 8		+3.7	+10.2	+86.9	+7.8	+6.8

field, completely missing the localized amplification induced by the real core geometry.

The differences in displacement fields are also evident in the deformed configurations reported in Fig. 16 for the CW model, and in Fig. 17 for the LW model. These highlight how the CW model captures the skin deflection caused by the local reduction in stiffness; indeed, the front view of the CW model deformed shape reveals a localized out-of-plane curvature of the upper skin, concentrated where no supporting cell is present below. LW model lacks this localized feature, offering a smooth and symmetric deflected profile due to the averaged stiffness representation.

This analysis highlights a fundamental shortcoming of homogenized core models when used in configurations affected by asymmetry, whether geometric or load-based. LW models based on core homogenization fail to detect stiffness discontinuities and variations and the associated local effects. CW modelling, thanks to its ability to resolve actual geometry and interfaces, provides a far more reliable prediction in such cases, making it the preferred option when accurate mechanical response is required.

Table 18
First eight natural frequencies. Case: regular honeycomb, $h = 20$ mm, t_s=1 mm.

	CW	Gibson	Nast	Shi-Tong	Kumar	Sorohan
	f [kHz]					
Mode 1	0.191	0.193	0.190	0.305	0.200	0.191
Mode 2	0.587	0.581	0.608	1.021	0.601	0.596
Mode 3	1.018	0.959	0.934	1.512	0.983	0.946
Mode 4	1.098	1.092	1.125	1.739	1.156	1.116
Mode 5	1.856	1.840	1.973	3.061	1.923	1.901
Mode 6	2.616	2.651	2.835	3.227	2.801	2.737
Mode 7	2.878	3.001	2.871	3.889	3.123	2.931
Mode 8	3.113	2.979	3.123	4.784	3.215	3.021

Table 19
Natural frequencies percent difference. Case: regular honeycomb, $h = 20$ mm, t_s=1 mm.

	CW	Gibson	Nast	Shi-Tong	Kumar	Sorohan
	Δ%f (w.r.t. CW)					
Mode 1	ref.	+1.0	−0.5	+59.7	+4.7	=
Mode 2		−1.0	+3.6	+73.9	+2.4	+1.5
Mode 3		−5.8	−8.3	+48.5	−3.4	−7.1
Mode 4		−0.5	+2.5	+58.4	+5.3	+1.6
Mode 5		−0.9	+6.3	+64.9	+3.6	+2.4
Mode 6		+1.3	+8.4	+23.4	+7.1	+4.6
Mode 7		+4.3	−0.2	+35.1	+8.5	+1.8
Mode 8		−4.3	+0.3	+53.7	+3.3	−3.0

Table 20
First eight natural frequencies. Case: regular honeycomb, $h = 40$ mm, t_s=1 mm.

	CW	Gibson	Nast	Shi Tong	Kumar	Sorohan
			f [kHz]			
Mode 1	0.316	0.315	0.308	0.458	0.335	0.312
Mode 2	0.831	0.775	0.750	1.194	0.793	0.762
Mode 3	0.906	0.861	0.925	1.394	0.907	0.897
Mode 4	1.711	1.624	1.718	2.003	1.778	1.692
Mode 5	2.566	2.460	2.309	3.273	2.563	2.387
Mode 6	2.726	2.540	2.502	3.576	2.578	2.518
Mode 7	2.784	2.622	2.911	4.165	2.793	2.757
Mode 8	3.872	3.693	4.112	4.158	4.020	3.911

Table 21
Natural frequencies percent difference. Case: regular honeycomb, $h = 40$ mm, t_s=1 mm.

	CW	Gibson	Nast	Shi-Tong	Kumar	Sorohan
	Δ%f (w.r.t. CW)					
Mode 1	ref.	−0.3	−2.5	+44.9	+6.0	−1.3
Mode 2		−6.7	−9.7	+43.7	−4.6	−8.3
Mode 3		−5.0	+2.1	+53.9	+0.1	−1.0
Mode 4		−5.1	+0.4	+17.1	+3.9	−1.1
Mode 5		−4.1	−10.0	+27.6	−0.1	−7.0
Mode 6		−6.8	−8.2	+31.2	−5.4	−7.6
Mode 7		−5.8	+4.6	+49.6	+0.3	−1.0
Mode 8		−4.6	+6.2	+7.4	+3.8	+1.0

4.3. Modal analysis

A detailed modal analysis comparing the high-fidelity component-wise model with layer-wise models based on different homogenization approaches reveals interesting insights into the dynamic behaviour prediction of sandwich structure with honeycomb core. The first analysed case refers to the regular honeycomb cell; the skins thickness ist$_s$ = 1 mm. Results in terms of first eight natural frequencies are reported in Table 16, Table 18, and Table 20 for the structures having h equal to 10 mm, 20 mm, and 40 mm, respectively. Table 17, Table 19, and Table 21,

Table 22
First eight natural frequencies. Case: non-regular honeycomb, $h = 10$ mm, t_s=1 mm.

	CW	Gibson	Nast	Kumar	Sorohan
	f [kHz]				
Mode 1	0.232	0.247	0.224	0.223	0.227
Mode 2	0.878	0.849	0.861	0.839	0.840
Mode 3	1.380	1.423	1.330	1.334	1.371
Mode 4	1.489	1.542	1.335	1.311	1.324
Mode 5	2.748	2.663	2.726	2.618	2.623
Mode 6	3.608	3.591	3.492	3.369	3.396
Mode 7	5.017	4.831	4.794	4.711	4.725
Mode 8	5.176	5.283	4.995	4.812	4.994

Table 23
Natural frequencies percent difference. Case: non-regular honeycomb, $h = 10$ mm, t_s=1 mm.

	CW	Gibson	Nast	Kumar	Sorohan
		Δ%f (w.r.t. CW)			
Mode 1	ref.	+6.5	−3.4	−3.9	−2.2
Mode 2		−3.3	−1.9	−4.4	−4.3
Mode 3		+3.1	−3.6	−3.3	−0.7
Mode 4		+3.6	−10.3	−12.0	−11.1
Mode 5		−3.1	−0.8	−4.7	−4.5
Mode 6		−0.5	−3.2	−6.6	−5.9
Mode 7		−3.7	−4.4	−6.1	−5.8
Mode 8		+2.1	−3.5	−7.0	−3.5

Table 24
First eight natural frequencies. Case: non-regular honeycomb, $h = 20$ mm, t_s=1 mm.

	CW	Gibson	Nast	Kumar	Sorohan
	f [kHz]				
Mode 1	0.412	0.458	0.384	0.382	0.392
Mode 2	1.287	1.331	1.096	1.104	1.158
Mode 3	1.432	1.333	1.367	1.313	1.316
Mode 4	2.337	2.366	2.157	2.085	2.127
Mode 5	4.378	4.046	3.946	3.966	3.977
Mode 6	4.783	4.593	4.132	3.978	4.261
Mode 7	4.687	5.388	4.216	4.151	4.279
Mode 8	5.780	5.462	5.308	5.005	5.079

Table 25
Natural frequencies percent difference. Case: non-regular honeycomb, $h = 20$ mm, t_s=1 mm.

	CW	Gibson	Nast	Kumar	Sorohan
	Δ%f (w.r.t. CW)				
Mode 1	ref.	+11.2	−6.8	−7.3	−4.9
Mode 2		+3.4	−14.8	−14.2	−10.0
Mode 3		−6.9	−4.5	−8.3	−8.1
Mode 4		+1.2	−7.7	−10.8	−9.0
Mode 5		−7.6	−9.9	−9.4	−9.2
Mode 6		−4.0	−13.6	−16.8	−10.9
Mode 7		+15.0	−10.0	−11.4	−8.7
Mode 8		−5.5	−8.2	−13.4	−12.1

shows the percentage error of the frequency prediction of the homogenised LW models with respect to the high-fidelity CW model. The Gibson, Nast, Kumar, and Sorohan models provide generally a good accuracy, especially for low frequency modes. The different models exhibit mode-dependent deviations, but in general the prediction is satisfying. A more trivial case is represented by the Shi-Tong model, that provides significantly higher in-plane stiffness values than the other models (see Table 9), and hence predicts natural frequencies that are

Table 26
First eight natural frequencies. Case: non-regular honeycomb, $h = 40$ mm, t_s=1 mm.

	CW	Gibson	Nast	Kumar	Sorohan
	f [kHz]				
Mode 1	0.679	0.762	0.604	0.593	0.624
Mode 2	1.061	1.050	0.875	0.868	0.926
Mode 3	2.020	1.782	1.866	1.764	1.765
Mode 4	3.475	3.295	3.056	2.879	2.969
Mode 5	3.857	3.599	3.162	3.122	3.357
Mode 6	4.066	4.413	3.265	3.246	3.516
Mode 7	6.001	5.271	5.610	5.202	5.213
Mode 8	7.718	7.038	6.733	6.441	6.583

Table 27
Natural frequencies percent difference. Case: non-regular honeycomb, $h = 40$ mm, t_s=1 mm.

	CW	Gibson	Nast	Kumar	Sorohan
	ref.	Δ%f (w.r.t. CW)			
Mode 1		+12.2	−11.0	−12.7	−8.1
Mode 2		−1.0	−17.5	−18.2	−12.7
Mode 3		−11.8	−7.6	−12.7	−12.6
Mode 4		−5.2	−12.1	−17.2	−14.6
Mode 5		−6.7	−18.0	−19.1	−13.0
Mode 6		+8.5	−19.7	−20.2	−13.5
Mode 7		−12.2	−6.5	−13.3	−13.1
Mode 8		−8.8	−12.8	−16.5	−14.7

markedly higher than those from the CW model. This pronounced overestimation across several modes indicates that the Shi-Tong approach predictive capability for dynamic response is largely unsatisfactory.

Another relevant observation is that, as the sandwich height increases from 10 mm to 20 mm and then to 40 mm, the overall bending stiffness of the structure increases due to the larger distance between the skins and the neutral axis. This increased stiffness results in a general rise in the natural frequencies for all modes. The CW model captures this trend accurately, and the LW models reflect similar increases; however, the percentage discrepancies between LW and CW predictions evolve with h. The results for the regular cell case are generally satisfactory, but they highlight considerable variability between the models as the sandwich height and the considered modes change. Specifically, the Gibson model shows a generally non-conservative trend for the lowest structure height, transitioning to an undefined situation for the intermediate height, and becoming conservative for larger values of h. In contrast, the models by Nast, Kumar, and Sorohan do not display a consistent trend, and their predictive accuracy varies significantly depending on the mode analyzed. These differences suggest that the results obtained may be specifically valid for the case under examination, raising concerns about their generalizability to other configurations or loading conditions. To verify this, it is necessary to also discuss the next case, involving an irregular cell.

In the non-regular cell configuration with a skin thickness of$t_s = 1$ mm, the modal frequencies exhibit a distinct pattern relative to the CW model. The irregular geometry introduces additional complexity in the deformational behaviour within the core, and this is reflected in the varied performance of the homogenization models. Results are provided in Table 22, Table 24, Table 26, for the natural frequencies of the cases having h equal to 10 mm, 20 mm, and 40 mm, respectively. Table 23, Table 25, and Table 27 report the percentage differences of the LW homogenized cases with respect to the CW reference. For example, in the lower modes the Gibson model tends to overpredict the frequency by about 6.5 % for mode 1, whereas the Nast, Kumar, and Sorohan models generally yield slightly lower or near-equal values for some modes. The percentage differences fluctuate with the mode order; mid-range modes

Table 28
First eight natural frequencies. Case: non-regular honeycomb, $h = 10$ mm, t_s=0.2 mm.

	CW	Gibson	Nast	Kumar	Sorohan
	f [kHz]				
Mode 1	0.178	0.218	0.147	0.146	0.157
Mode 2	0.623	0.624	0.586	0.580	0.586
Mode 3	1.114	1.077	0.806	0.797	0.892
Mode 4	1.081	1.275	0.901	0.891	0.957
Mode 5	2.011	2.088	1.898	1.867	1.902
Mode 6	2.911	3.256	2.465	2.424	2.590
Mode 7	3.775	3.539	2.926	2.883	3.181
Mode 8	3.876	4.163	3.007	2.997	3.380

Table 29
Natural frequencies percent difference. Case: non-regular honeycomb, $h = 10$ mm, t_s=0.2 mm.

	CW	Gibson	Nast	Kumar	Sorohan
	ref.	Δ%f (w.r.t. CW)			
Mode 1		+22.8	−17.5	−18.1	−11.5
Mode 2		+0.1	−5.9	−6.8	−5.9
Mode 3		−3.3	−27.7	−28.4	−20
Mode 4		+17.9	−16.7	−17.6	−11.5
Mode 5		+3.8	−5.6	−7.2	−5.4
Mode 6		+11.9	−15.3	−16.7	−11
Mode 7		−6.2	−22.5	−23.6	−15.7
Mode 8		+7.4	−22.4	−22.7	−12.8

Table 30
First eight natural frequencies. Case: non-regular honeycomb, $h = 20$ mm, t_s=0.2 mm.

	CW	Gibson	Nast	Kumar	Sorohan
	f [kHz]				
Mode 1	0.297	0.371	0.222	0.219	0.251
Mode 2	0.915	0.832	0.615	0.604	0.702
Mode 3	0.936	0.912	0.848	0.836	0.849
Mode 4	1.761	2.018	1.334	1.306	1.477
Mode 5	3.022	2.702	2.250	2.189	2.440
Mode 6	3.185	3.001	2.274	2.261	2.723
Mode 7	3.649	3.513	2.716	2.646	2.760
Mode 8	4.567	4.701	3.549	3.442	3.824

Table 31
Natural frequencies percent difference. Case: non-regular honeycomb, $h = 20$ mm, t_s=0.2 mm.

	CW	Gibson	Nast	Kumar	Sorohan
	Δ%f (w.r.t. CW)				
Mode 1	ref.	+24.9	−25.3	−26.4	−15.4
Mode 2		−9.1	−32.8	−34.0	−23.3
Mode 3		−2.6	−9.4	−10.7	−9.2
Mode 4		+14.6	−24.2	−25.8	−16.1
Mode 5		+10.6	−25.5	−27.6	−19.3
Mode 6		−5.8	−28.6	−29.0	−14.5
Mode 7		−3.7	−25.6	−27.5	−24.3
Mode 8		+ 2.9	−22.3	−24.6	−16.3

show both over- and underestimations depending on the balance between in-plane and shear stiffness captured by each homogenized model. The irregular cell geometry inherently alters the effective stiffness of the core, and the predictive accuracy in this case seems more affected than the regular case. As the core geometry deviates from an ideal symmetric arrangement, the structural behaviour approximation becomes more sensitive to the accurate representation of both the in-plane moduli and the shear properties. The discrepancies observed

Table 32
First eight natural frequencies. Case: non-regular honeycomb, $h = 40$ mm, t_s=0.2 mm.

	CW	Gibson	Nast	Kumar	Sorohan
		f [kHz]			
Mode 1	0.487	0.572	0.328	0.320	0.396
Mode 2	0.747	0.621	0.469	0.456	0.534
Mode 3	1.327	1.208	1.140	1.115	1.137
Mode 4	2.644	2.013	1.705	1.659	1.823
Mode 5	2.714	2.633	1.740	1.694	2.151
Mode 6	3.095	2.755	1.876	1.808	2.199
Mode 7	4.205	3.810	3.515	3.439	3.549
Mode 8	5.072	3.954	3.563	3.502	3.656

Table 33
Natural frequencies percent difference. Case: non-regular honeycomb, $h = 40$ mm, t_s=0.2 mm.

	CW	Gibson	Nast	Kumar	Sorohan
	Δ%f (w.r.t. CW)				
Mode 1	ref.	+17.3	–32.7	–34.4	–18.7
Mode 2		–16.9	–37.3	–39.0	–28.5
Mode 3		–8.9	–14.0	–15.9	–14.3
Mode 4		–23.9	–35.5	–37.3	–31.1
Mode 5		–3.0	–35.9	–37.6	–20.8
Mode 6		–11.0	–39.4	–41.6	–28.9
Mode 7		–9.4	–16.4	–18.2	–15.6
Mode 8		–22.0	–29.7	–31.0	–27.9

Table 34
First eight natural frequencies. Case: non-regular honeycomb, $h = 10$ mm, t_s=2 mm.

	CW	Gibson	Nast	Kumar	Sorohan
			f [kHz]		
Mode 1	0.229	0.236	0.230	0.229	0.229
Mode 2	0.886	0.836	0.860	0.834	0.834
Mode 3	1.354	1.339	1.343	1.310	1.312
Mode 4	1.591	1.645	1.526	1.525	1.542
Mode 5	2.758	2.577	2.701	2.569	2.570
Mode 6	3.426	3.334	3.440	3.285	3.290
Mode 7	4.912	4.563	4.876	4.544	4.546
Mode 8	5.230	5.106	5.515	5.087	5.089

between the LW models and the CW reference underscore that even small errors in the equivalent properties can lead to measurable changes in the dynamic response.

Similar to the regular case, an increase in h causes a shift in the modal frequencies, with the CW model showing higher values as the structure becomes more rigid. However, the percentage differences between the LW models and the CW model in the non-regular case reveal that the relative error is mode-dependent. Lower-order modes, which are primarily governed by the overall bending stiffness, see Appendix A, display smaller relative differences, whereas modes that involve significant torsional or extensional deformation tend to show larger discrepancies. This further indicates the sensitivity the homogenized models could have on the specific deformational response of each mode, further highlighting the difficulty in extending these models to general studies.

To thoroughly explore the potential and limitations of predictive models based on core homogenization, it is necessary to take a further step forward. Indeed, as shown in Section 4.1 for the static case, the fact that such models neglect some global structural parameters of the sandwich, such as the skin thickness, makes their predictive capability highly dependent on the specific case under consideration. To verify this also in the context of modal analysis, two additional sets of analyses were performed for each model considered; the first set considers the same structures with the non-regular honeycomb previously discussed, but with a skin thickness$t_s = 0.2$ mm. With such a reduction of the skin thickness, the overall stiffness of the sandwich structure decreases markedly. Results in terms of natural frequencies for this case are reported in Table 28, Table 30, and Table 32, for the case of h equal to 10 mm, 20 mm, and 40 mm, respectively. In these scenarios, the core contribution becomes more pronounced, and the dynamic response is highly sensitive to the accuracy of the homogenized equivalent

Table 35
Natural frequencies percent difference. Case: non-regular honeycomb, $h = 10$ mm, t_s=2 mm.

	CW	Gibson	Nast	Kumar	Sorohan
	ref.		Δ%f (w.r.t. CW)		
Mode 1		+3.1	+0.4	–0.1	–0.1
Mode 2		–5.7	–2.9	–5.9	–5.9
Mode 3		–1.1	–0.8	–3.3	–3.1
Mode 4		+3.4	–4.1	–4.1	–3.1
Mode 5		–6.6	–2.1	–6.9	–6.8
Mode 6		–2.7	+0.4	–4.1	–4.0
Mode 7		–7.1	–0.7	–7.5	–7.5
Mode 8		–2.4	+5.5	–2.7	–2.7

Table 36
First eight natural frequencies. Case: non-regular honeycomb, $h = 20$ mm, t_s=2 mm.

	CW	Gibson	Nast	Kumar	Sorohan
	f [kHz]				
Mode 1	0.454	0.469	0.437	0.431	0.436
Mode 2	1.466	1.392	1.337	1.334	1.367
Mode 3	1.566	1.507	1.463	1.387	1.388
Mode 4	2.478	2.309	2.319	2.201	2.214
Mode 5	4.691	4.107	4.427	4.089	4.091
Mode 6	5.359	5.202	4.822	4.808	4.985
Mode 7	5.401	5.364	5.032	5.026	5.094
Mode 8	5.939	5.860	5.458	5.048	5.068

Table 37
Natural frequencies percent difference. Case: non-regular honeycomb, $h = 20$ mm, t_s=2 mm.

	CW	Gibson	Nast	Kumar	Sorohan
	ref.	Δ%f (w.r.t. CW)			
Mode 1		+3.2	–3.8	–5.0	–4.1
Mode 2		–5.1	–8.8	–9.0	–6.8
Mode 3		–3.8	–6.6	–11.4	–11.4
Mode 4		–6.8	–6.4	–11.2	–10.6
Mode 5		–12.5	–5.6	–12.8	–12.8
Mode 6		–2.9	–10.0	–10.3	–7.0
Mode 7		–0.7	–6.8	–7.0	–5.7
Mode 8		–1.3	–8.1	–15.0	–14.7

Table 38
First eight natural frequencies. Case: non-regular honeycomb, $h = 40$ mm, t_s=2 mm.

	CW	Gibson	Nast	Kumar	Sorohan
	f [kHz]				
Mode 1	0.774	0.809	0.727	0.709	0.724
Mode 2	1.235	1.254	1.107	1.103	1.144
Mode 3	2.254	1.912	2.049	1.909	1.909
Mode 4	3.701	3.280	3.343	3.089	3.123
Mode 5	4.545	4.424	3.988	3.959	4.233
Mode 6	4.616	5.114	4.149	4.127	4.211
Mode 7	6.555	5.538	6.075	5.523	5.524
Mode 8	8.165	6.891	7.317	6.631	6.680

Table 39
Natural frequencies percent difference. Case: non-regular honeycomb, $h = 40$ mm, t_s=2 mm.

	CW	Gibson	Nast	Kumar	Sorohan
	ref.	Δ%f (w.r.t. CW)			
Mode 1		+4.6	−6.1	−8.4	−6.4
Mode 2		+1.6	−10.3	−10.7	−7.4
Mode 3		−15.2	−9.1	−15.3	−15.3
Mode 4		−11.4	−9.7	−16.5	−15.6
Mode 5		−2.7	−12.2	−12.9	−6.9
Mode 6		+10.8	−10.1	−10.6	−8.8
Mode 7		−15.5	−7.3	−15.8	−15.7
Mode 8		−15.6	−10.4	−18.8	−18.2

properties, see Table 29, Table 31, and Table 33. The LW models, when compared to the CW benchmark, show larger percentage differences in modal frequencies. For instance, mode 1 in the Gibson model can be overestimated by more than 20 %, while models such as Nast and Kumar tend to underpredict certain modes by a similar magnitude. These discrepancies highlight that the thinner skin accentuates any inaccuracies in the core representation, making the prediction of modal parameters particularly challenging. The influence of a thin skin is observed across all mode orders, but the discrepancies are most severe in modes where the bending deformation and extensional behaviour are predominant. Furthermore, as h increases, the sensitivity to these inaccuracies becomes more critical. The reduced skin stiffness amplifies the effect of any error in the computed core stiffness, leading to an overall dynamic response that diverges more significantly from the CW model.

Ultimately, reducing the skin thickness confers greater significance to the equivalent mechanical properties of the core, resulting in an increase in the error compared to the case with$t_s = 1$ mm. To verify this hypothesis, a second set of simulations was conducted, in which the skin thickness was increased to t_s=2 mm. Indeed, when the skin thickness is increased, the overall bending stiffness of the sandwich structure is enhanced. This results in higher modal frequencies, as observed in the CW model, see results reported in Table 34, Table 36, and Table 38 for the cases having h equal to 10 mm, 20 mm, and 40 mm, respectively. It is noteworthy, however, that the case with $h = 10$ mm, in the high-fidelity CW estimates, exhibits frequencies comparable to or slightly lower than the reference case with the same height and$t_s = 1$, contradicting the expected increase in stiffness. In this case, it is clear that the thickening of the skins also introduces mass increases that counterbalance its stiffening effect. In general, the LW models tend to converge more closely to the CW predictions, again with an error amplifying effect of the structure height h, see Table 35, Table 37, Table 39. The percentage differences between the models are reduced, with most modes exhibiting discrepancies within a few percent. This improved agreement can be attributed to the fact that the thicker skins contribute dominantly to the global stiffness, thereby diminishing the relative impact of any inaccuracies in the homogenized core properties. For instance, in the modes where bending is predominant, the increased stiffness of the skins ensures that the LW models predict frequencies that align well with the CW model. Again, Gibson model does not exhibit a definite trend, with over- and underestimated predictions depending on the considered mode. The overall trend indicates that as the contribution of the skins becomes more significant, the dynamic response becomes less sensitive to variations in the core equivalent properties.

To generalize, the modal analysis results emphasize that the accuracy of the LW models in predicting the natural frequencies of sandwich structures is highly dependent on both the homogenization technique and the global geometric parameters. A careful balance between capturing the core effective stiffness and accounting for the dominant contribution of the skins is essential to achieve reliable predictions across a range of configurations. This indicates that a general conclusion on accuracy of simplified models to be applied to each honeycomb core sandwich structure cannot be formalized, as this depends on each specific study case. Homogenized models remains useful hence for conceptual investigations, to qualitatively identify main trends of the structural responses. On the other hand, CW models can be considered as high-fidelity tools to support the study of mechanical behaviour of complex structures and their engineering development and integration [42].

4.4. Key findings and practical guidelines

The comparative investigation carried out in this work provides a set of general guidelines that can support the design and analysis of sandwich structures with honeycomb cores. The following observations translate the results into practical implications for modelling choices in engineering contexts. First, analytical homogenization models preserve their role in early-stage design, where rapid evaluations of global orthotropic behavior are sufficient. They allow engineers to perform preliminary assessments and parametric studies with limited modelling or computational effort. However, the simplifications they adopt inevitably restrict their predictive capability. In particular, when skin properties or local geometric variations are expected to affect global stiffness and vibration response, homogenization-based models may yield misleading results if taken as the sole reference. Their value therefore lies in providing quick initial estimates, not in supporting final design decisions. Second, the CW approach emerges as the natural benchmark for design activities that demand reliability and physical consistency. By explicitly resolving the honeycomb architecture, CW models are able to capture the heterogeneous stiffness distribution that critically governs bending, torsion, and modal behavior. Importantly, the efficiency of CW formulations within the CUF makes them viable for engineering practice: they retain accuracy comparable to detailed 3D simulations while exhibiting significant reductions in required degrees of freedom. This was already discussed and demonstrated in ref. [30], for honeycomb structures. By enabling a refined 1D representation of both core and skins without homogenization, CUF-CW models can reproduce three-dimensional stress fields with a dramatically reduced number of degrees of freedom. This efficiency does not compromise predictive capabilities, as CUF models are able to capture both global and local mechanical behaviors, including through-the-thickness stress distributions and interfaces deformations. These features make the CUF-based CW strategy particularly attractive for high-fidelity simulations of sandwich structures, where classical 3D modeling would otherwise entail prohibitive computational costs.

These guidelines help delineate the proper balance between efficiency and fidelity: homogenization supports exploration, while CW modelling ensures reliability. This dual perspective enables a more rational and cost-effective use of numerical methods in the design of advanced sandwich structures.

5. Conclusions

This paper has shown that the mechanical response of sandwich structures with honeycomb cores is highly sensitive to the specific geometry, arrangement, and local stiffness distribution of the cellular architecture. Analytical homogenization models, although widely used to approximate orthotropic equivalent properties, often fail to capture such local effects. This leads to a substantial dependency of the results not only on the global parameters of the unit cell but also on localized features that affect stiffness variations. When implemented within a CUF-based Layer-Wise formulation, homogenized properties can be employed to efficiently perform structural simulations with reduced computational cost. However, the analysis conducted in this study clearly highlights that such models are suitable primarily for preliminary or qualitative assessments. In practical design scenarios the LW approach could likely provide misleading predictions. In such cases, a Component-Wise formulation, capable of resolving the real geometry and interfaces kinematics, becomes essential to obtain physically

meaningful results. The CW implementation within Carrera Unified Formulation demonstrated excellent performance in terms of resolution-to-cost ratio. Despite being geometrically explicit, the model maintains a relatively low number of degrees of freedom compared to full 3D simulations, offering an effective compromise between fidelity and efficiency. Additional limitations of the LW model emerge when considering realistic scenarios involving geometric or material heterogeneity within the honeycomb core, such as regions with different cell sizes, shapes, or material compositions. Under these conditions, homogenization procedures cannot be used, as the physical interpretation of the resulting equivalent properties is no longer reliable.

Future developments will focus on establishing systematic procedures to identify the most appropriate homogenization model for a given sandwich structural model. In particular, sensitivity analyses will be carried out to quantify the influence of geometric and material variations on the mechanical response predicted by LW models. This will contribute to the formulation of more robust guidelines for the use of homogenized approaches in sandwich structure design, and to the general characterization of the mechanical behaviour of architected cellular cores.

CRediT authorship contribution statement

Erasmo Carrera: Conceptualization, Data curation, Formal analysis, Funding acquisition, Investigation, Methodology, Supervision, Writing – original draft. **Karim Abu Salem:** Conceptualization, Formal analysis, Investigation, Methodology, Visualization, Writing – original draft. **Riccardo Augello:** Data curation, Investigation, Validation, Writing – review & editing.

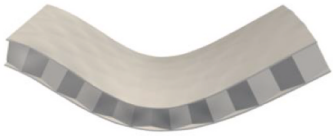
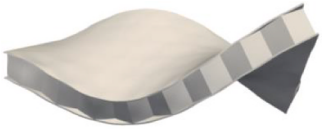
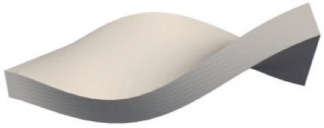
Declaration of competing interest

The authors declare that they have no known competing financial interests or personal relationships that could have appeared to influence the work reported in this paper.

The author is an Editorial Board Member/Editor-in-Chief/Associate Editor/Guest Editor for *Composite Structures* and was not involved in the editorial review or the decision to publish this article.

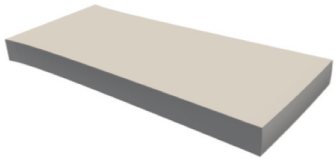
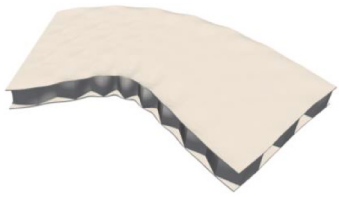
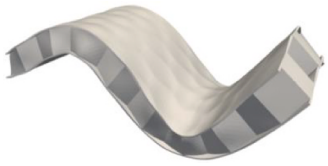
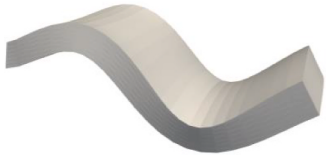
Appendix A

Mode shapes for irregular honeycomb case ($h = 20$ mm, $t_s = 1$ mm).

Mode	Description	Mode Shape CW	Mode Shape LW (Kumar)
1	Bending		
2	In-planebending		
3	Torsion		
4	Middlebending		
5	Doubletorsion		

(*continued on next page*)

(*continued*)

Mode	Description	Mode Shape CW	Mode Shape LW (Kumar)
6	Extensional		
7	In-planemiddle bending		
8	Doublebending		

Data availability

Data will be made available on request.

References

[1] Ramnath BV, Alagarraja K, Elanchezhian C. Review on sandwich composite and their applications. Mater Today Proc 2019;16:859–64. https://doi.org/10.1016/j.matpr.2019.05.169.

[2] Feng Y, Qiu H, Gao Y, Zheng H, Tan J. Creative design for sandwich structures: a review. Int J Adv Rob Syst 2020;17(3). https://doi.org/10.1177/1729881420921327.

[3] Solak A. Bioinspired honeycomb sandwich structures for enhanced hail impact resistance. Mech Adv Mater Struct 2025;32(2):194–202. https://doi.org/10.1080/15376494.2024.2341303.

[4] Sun Z, Shi S, Guo X, Hu X, Chen H. On compressive properties of composite sandwich structures with grid reinforced honeycomb core. Compos B Eng 2016;94:245–52. https://doi.org/10.1016/j.compositesb.2016.03.054.

[5] Wang D, Xu P, Yang C, Xiao X, Che Q. Crashing performance and multi-objective optimization of honeycomb-filled thin-walled energy absorber with axisymmetric thickness. Mech Adv Mater Struct 2023;30(11):2203–20. https://doi.org/10.1080/15376494.2022.2053765.

[6] Zhao X, Wei L, Wen D, Zhu G, Yu Q, Ma ZD. Bending response and energy absorption of sandwich beams with novel auxetic honeycomb core. Eng Struct 2021;247:113204. https://doi.org/10.1016/j.engstruct.2021.113204.

[7] Li S, Yang R, Sun S, Niu B. Advances in the analysis of honeycomb structures: a comprehensive review. Compos B Eng 2025;112208. https://doi.org/10.1016/j.compositesb.2025.112208.

[8] Roy R, Kweon JH, Choi JH. Meso-scale finite element modeling of NomexTM honeycomb cores. Adv Compos Mater 2014;23(1):17–29. https://doi.org/10.1080/09243046.2013.862382.

[9] Onyibo EC, Safaei B. Application of finite element analysis to honeycomb sandwich structures: a review. Reports in Mechanical Engineering 2022;3(1):192–209. https://doi.org/10.31181/rme200230320220.

[10] Yun J, Ryu S, Kim J, Kim Y, Kim DW. Equivalent modeling for the prediction of mechanical behaviors of composite sandwich structures with thick cell walls. Compos Struct 2025;119162. https://doi.org/10.1016/j.compstruct.2025.119162.

[11] Yang JS, Li DL, Ma L, Zhang SQ, Schröder KU, Schmidt R. Numerical static and dynamic analyses of improved equivalent models for corrugated sandwich structures. Mech Adv Mater Struct 2019;26(18):1556–67. https://doi.org/10.1080/15376494.2018.1444232.

[12] Ahmed, N., Zafar, N., & Janjua, H. Z. (2019, January). Homogenization of honeycomb core in sandwich structures: A review. In *2019 16th International Bhurban Conference on Applied Sciences and Technology (IBCAST IEEE)* (pp. 159-173), doi: 10.1109/IBCAST.2019.8667144.

[13] Zhang X, Yin X, Xu C, Li W. Study on the equivalent model considering in-plane and out-of-plane mechanical properties for a curved sandwich structure with square honeycomb core. Mech Adv Mater Struct 2024;1–20. https://doi.org/10.1080/15376494.2024.2422577.

[14] Moeini M, Begon M, Lévesque M. Numerical homogenization of a linearly elastic honeycomb lattice structure and comparison with analytical and experimental results. Mech Mater 2022;167:104210. https://doi.org/10.1016/j.mechmat.2022.104210.

[15] Gibson J, Ashby M. *Cellular Solids: Structure and Properties*. Cambridge University Press 1997. https://doi.org/10.1017/CBO9781139878326.

[16] Schwingshackl CW, Aglietti GS, Cunningham PR. Determination of honeycomb material properties: existing theories and an alternative dynamic approach. J Aerosp Eng 2006;19(3):177–83. https://doi.org/10.1061/(ASCE)0893-1321(2006)19:3(177).

[17] Sather, E., & Krishnamurthy, T. (2019). An analytical method to calculate effective elastic properties of general multifunctional honeycomb cores in sandwich composites (*NASA Technical Memorandum TM-2019-220275*), available at: https://ntrs.nasa.gov/citations/20190025271.

[18] Burton WS, Noor AK. Assessment of continuum models for sandwich panel honeycomb cores. Comput Methods Appl Mech Eng 1997;145(3–4):341–60. https://doi.org/10.1016/S0045-7825(96)01196-6.

[19] Jiang D, Zhang D, Fei Q, Wu S. An approach on identification of equivalent properties of honeycomb core using experimental modal data. Finite Elem Anal Des 2014;90:84–92. https://doi.org/10.1016/j.finel.2014.06.006.

[20] Li YM, Hoang MP, Abbes B, Abbes F, Guo YQ. Analytical homogenization for stretch and bending of honeycomb sandwich plates with skin and height effects. Compos Struct 2015;120:406–16. https://doi.org/10.1016/j.compstruct.2014.10.028.

[21] Malek S, Gibson L. Effective elastic properties of periodic hexagonal honeycombs. Mech Mater 2015;91:226–40. https://doi.org/10.1016/j.mechmat.2015.07.008.

[22] Mukhopadhyay T, Adhikari S. Equivalent in-plane elastic properties of irregular honeycombs: an analytical approach. Int J Solids Struct 2016;91:169–84. https://doi.org/10.1016/j.ijsolstr.2015.12.006.

[23] Ahmed N, Zafar N, Janjua HZ. January). Homogenization of honeycomb core in sandwich structures: a review. In: In *2019 16th International Bhurban Conference on Applied Sciences and Technology (IBCAST)*; 2019. https://doi.org/10.1109/IBCAST.2019.8667144.

[24] Catapano A, Montemurro M. A multi-scale approach for the optimum design of sandwich plates with honeycomb core. Part I: homogenisation of core properties.

Compos Struct 2014;118:664–76. https://doi.org/10.1016/j.compstruct.2014.07.057.
[25] Carrera E, Cinefra M, Petrolo M, Zappino E. Finite element analysis of structures through unified formulation. John Wiley & Sons; 2014.
[26] Zhou Z, Chen M, Li Y. Application scope studies of analytical methods based on the equivalent single-layer and layerwise theories for vibration analysis of symmetric sandwich plates. Acta Mech 2023;234(2):377–401. https://doi.org/10.1007/s00707-022-03392-3.
[27] Carrera E. Theories and finite elements for multilayered plates and shells: a unified compact formulation with numerical assessment and benchmarking. Arch Comput Meth Eng 2003;10:215–96. https://doi.org/10.1007/BF02736224.
[28] Moreira RAS, Rodrigues JD. A layerwise model for thin soft core sandwich plates. Comput Struct 2006;84(19–20):1256–63. https://doi.org/10.1016/j.compstruc.2006.01.020.
[29] Hachemi M. Layer-wise solutions for variable stiffness composite laminated sandwich plate using curvilinear fibers. Mech Adv Mater Struct 2022;29(26):5460–77. https://doi.org/10.1080/15376494.2021.1956028.
[30] Abu Salem K, Augello R, Carrera E. Component-wise modelling of core and skin in sandwich structures using a single refined beam finite element. Mech Adv Mater Struct 2025;1–14. https://doi.org/10.1080/15376494.2025.2458237.
[31] Pagani, A. (2015). Component-wise models for static, dynamic and aeroelastic analyses of metallic and composite aerospace structures, *PhD Thesis*, Politecnico di Torino, available at: https://tesidottorato.depositolegale.it/bitstream/20.500.14242/108661/1/PhD_Thesis_AP.compressed.pdf.
[32] Zappino E, Viglietti A, Carrera E. The analysis of tapered structures using a component-wise approach based on refined one-dimensional models. Aerosp Sci Technol 2017;65:141–56. https://doi.org/10.1016/j.ast.2017.02.004.
[33] Nast, E. (1997). On honeycomb-type core moduli. 38th AIAA Structures, Structural Dynamics, and Materials Conference, 07-10 April 1997, Kissimmee, USA, Doi: 10.2514/6.1997-1178.
[34] Shi G, Tong P. The derivation of equivalent constitutive equations of honeycomb structures by a two scale method. Comput Mech 1995;15(5):395–407. https://doi.org/10.1007/BF00350354.
[35] Kumar A, Muthu N, Narayanan RG. Equivalent orthotropic properties of periodic honeycomb structure: strain-energy approach and homogenization. Int J Mech Mater Des 2023;19(1):137–63. https://doi.org/10.1007/s10999-022-09620-x.
[36] Sorohan S, Constantinescu DM, Sandu M, Sandu AG. On the homogenization of hexagonal honeycombs under axial and shear loading. Part I: Analytical formulation for free skin effect. Mech Mater 2018;119:74–91. https://doi.org/10.1016/j.mechmat.2017.09.003.
[37] Sorohan Ş, Sandu M, Sandu A, Constantinescu DM. Finite element models used to determine the equivalent in-plane properties of honeycombs. Mater Today Proc 2016;3(4):1161–6. https://doi.org/10.1016/j.matpr.2016.03.013.
[38] Bargmann S, Klusemann B, Markmann J, Schnabel JE, Schneider K, Soyarslan C, et al. Generation of 3D representative volume elements for heterogeneous materials: a review. Prog Mater Sci 2018;96:322–84. https://doi.org/10.1016/j.pmatsci.2018.02.003.
[39] Qiu C, Guan Z, Jiang S, Li Z. A method of determining effective elastic properties of honeycomb cores based on equal strain energy. Chin J Aeronaut 2017;30(2):766–79. https://doi.org/10.1016/j.cja.2017.02.016.
[40] Montemurro M, Catapano A, Doroszewski D. A multi-scale approach for the simultaneous shape and material optimisation of sandwich panels with cellular core. Compos B Eng 2016;91:458–72. https://doi.org/10.1016/j.compositesb.2016.01.030.
[41] Guan C, Lou R, Chen Y, Qin C, Shi Z, Liang L, et al. A homogenization method for natural frequencies and damping of sandwich panels based on representative volume elements. Compos Struct 2024;329:117740. https://doi.org/10.1016/j.compstruct.2023.117740.
[42] Carrera E, Augello R, Abu Salem K. Evaluation of the effects of different materials on the dynamic properties of thin-walled metamaterial structures. Mech Adv Mater Struct 2024;1–16. https://doi.org/10.1080/15376494.2024.2434194.